

Durham Research Online

Deposited in DRO:

19 October 2015

Version of attached file:

Accepted Version

Peer-review status of attached file:

Peer-reviewed

Citation for published item:

Peters, J.L. and Benetti, S. and Dunlop, P. and Ó Cofaigh, C. (2015) 'Maximum extent and dynamic behaviour of the last British-Irish Ice Sheet west of Ireland.', *Quaternary science reviews.*, 128 . pp. 48-68.

Further information on publisher's website:

<http://dx.doi.org/10.1016/j.quascirev.2015.09.015>

Publisher's copyright statement:

© 2015 This manuscript version is made available under the CC-BY-NC-ND 4.0 license
<http://creativecommons.org/licenses/by-nc-nd/4.0/>

Additional information:

Use policy

The full-text may be used and/or reproduced, and given to third parties in any format or medium, without prior permission or charge, for personal research or study, educational, or not-for-profit purposes provided that:

- a full bibliographic reference is made to the original source
- a [link](#) is made to the metadata record in DRO
- the full-text is not changed in any way

The full-text must not be sold in any format or medium without the formal permission of the copyright holders.

Please consult the [full DRO policy](#) for further details.

1 Maximum extent and dynamic behaviour of the last British-Irish Ice Sheet west
2 of Ireland

3 **Jared Lee Peters**^{1*}, Sara Benetti¹, Paul Dunlop¹, Colm Ó Cofaigh²

4 * Corresponding author. Email: Peters-J@email.ulster.ac.uk

5 ¹*School of Environmental Sciences, University of Ulster, Cromore Road, Coleraine, BT52 1SA,*
6 *Northern Ireland, UK*

7 ²*Department of Geography, Durham University, Durham, DH1 3LE, UK*

8 **Abstract**

9 A complete reconstruction of the last British-Irish Ice Sheet (BIIS) is hindered by uncertainty
10 surrounding its offshore extent and dynamic behaviour. This study addresses this problem by
11 reconstructing the depositional history of four sediment cores taken from a series of sinuous
12 glacial sediment ridges on the continental shelf west of Ireland. We present new geomorphic,
13 sedimentary and micropaleontological data that record a maximum westward BIIS extent that was at
14 least 80 km farther offshore from any previous estimates. The data suggests that a large ice shelf
15 formed over parts of the shelf prior to retreat. This new data increases the areal extent of grounded
16 BIIS ice by ~6,700 km² from previous estimates, which represents a ~3% increase in the Irish Sector
17 of the ice sheet. Three new AMS radiocarbon dates demonstrate for the first time that the BIIS
18 advanced to the shelf edge during last glaciation (Late Midlandian/Late Devensian), with ice advance
19 onto the Porcupine Bank occurring after 24,720±260 yr Cal. BP. Deglaciation was complete by
20 19,182±155 yr Cal. BP, thus constraining BIIS occupation over the Porcupine Bank to less than 5,500
21 years. Estimated retreat rates of marine-terminating ice across the shelf range from ~70-180 myr⁻¹.

22 **Key words**

23 British-Irish Ice Sheet; marine-terminating ice margin; maximum extent; Porcupine Bank; continental
24 shelf; ice shelf; radiocarbon; sedimentology; benthic foraminifera; geomorphology

1. Introduction

Despite more than a century of investigation, there remains much about the last (Midlandian) British-Irish Ice Sheet (BIIS) that is poorly understood, particularly with respect to its marine-terminating margins, which would likely have been crucial to ice sheet dynamics and mass balance given the sensitivity of such margins to environmental forcing (Rott et al., 2002; Rignot et al., 2004; Scambos et al., 2004; Domack et al., 2005; Pfeffer, 2007; Pritchard et al., 2009; Glasser et al., 2011). Additionally, the BIIS has been proposed as a possible analogue for sections of the West Antarctic Ice Sheet (WAIS) (Clark et al., 2012a) that are thought to be potentially unstable (Lowe and Anderson, 2003; Gladstone et al., 2012; Park et al., 2013; Ren et al. 2013), highlighting the importance of developing a better understanding of marine-based ice masses. This research is the first to produce dated sedimentary and geomorphological evidence of what is likely the westernmost extent of the last BIIS's marine-terminating margin.

Previous investigations of the last glaciation of the Irish continental shelf using marine geophysical data have identified large arcuate ridges north and west of Ireland (King et al., 1998; Sejrup et al., 2005; Benetti et al., 2010; Dunlop et al., 2010; Ó Cofaigh et al., 2010; Fig. 1a). These ridges were first interpreted by King et al. (1998) as end moraines (Fig. 1a) and Sejrup et al. (2005) subsequently confirmed this interpretation on the basis of seismic data. More recently, detailed geomorphic analyses have been completed on the Irish continental shelf west and north of Donegal Bay and the Malin Sea. This research has documented nested end- and recessional moraines, lateral moraines, drumlin swarms, and extensive areas of iceberg scouring that confirm the presence of grounded, marine-terminating ice lobes on the continental shelf (Benetti et al., 2010; Dunlop et al., 2010; Ó Cofaigh et al., 2010).

Despite these geomorphologic advancements, no analyses of the glacial sedimentology or palaeoenvironment have been completed west of Ireland. Furthermore, no previous research has dated the advance of the BIIS onto the continental shelf west of Ireland. This research coordinates

new geomorphology that addresses a previously uninvestigated area of the glaciated North Atlantic margin using multibeam swath bathymetric data with sedimentary and micropaleontological data gathered from vibro-cores. This study employs these data to elucidate the chronology and behaviour of the BIIS west of Ireland. The bathymetric and sedimentary data are collected from a series of sediment ridges on the northern Porcupine Bank and Slyne Trough, offshore western Ireland, (Fig. 1b). These landforms are situated on the outer continental shelf, ~60 km northwest (i.e. farther offshore) of the large moraine offshore of County Galway (referred to in this paper as the Galway Lobe Moraine) described by Clark et al. (2012a) (Fig. 1).

The Porcupine Bank itself forms a dome-like westward projection of the Irish continental shelf, situated north of the Porcupine Seabight (Fig. 1). Water depths across the Porcupine Bank range from ~155-200 m bsl and it is made distinct from the continuous continental shelf by the Slyne Trough (Fig. 1), a relatively low relief, N-S trending 'saddle' formed by a Mesozoic sedimentary basin (Murphy and Croker, 1992). These features constitute a relatively complex shelf bathymetry that was likely to have affected BIIS behaviour. Previous studies have investigated the evolution of cold-water coral mounds that occupy deeper water flanking the Porcupine Bank, some of which identified intervals of IRD (e.g., De Haas et al., 2009; Heindel et al., 2010; Smeulders et al., 2014); however no palaeoglaciological investigations have previously been completed on the Porcupine Bank and the glaciological significance of the IRD is uninvestigated.

The sediment ridges across the Porcupine Bank and Slyne Trough have not been previously studied. In this paper we present a series of data that indicate that these ridges are glacial in origin. We also present several AMS radiocarbon dates that offer the first chronologic constraints for ice advance across the shelf, which indicate BIIS advance during the last (late Midlandian) glaciation (MIS 2). This study area was selected for three reasons: (1) the origin of the ridges was unknown, (2) bathymetric data coverage is precise and complete in this area and (3) previous studies of the Irish continental margin (e.g. Benetti et al., 2010; Ó Cofaigh et al., 2010; Sacchetti et al., 2012) call into question the western extent of the last BIIS and its behaviour along its marine termini. These

properties allowed us to address the aims of this study, which were to: (1) identify BIIS maximum extent west of Ireland, (2) provide the first age constraints for the timing of this advance, (3) identify depositional mechanisms and ice-proximal palaeoenvironmental signals that reveal BIIS behaviour, and (4) constrain the timeframe of BIIS marine margin retreat west of Ireland.

2. Methods

This research employs multibeam swath bathymetric raster data collected by the Irish National Seafloor Survey (INSS)—now the Integrated Mapping for the Sustainable Development of Ireland’s Marine Resource (INFOMAR) programme—to investigate the western margin of the Irish continental shelf. The data were collected in 2000 and 2001 by the *RSV Siren* using a hull-mounted Simrad© EM1002 multibeam system. The data are compiled into a series of 25 m resolution bathymetric rasters using a Geographic Information System (GIS) to analyse the seafloor geomorphology and to target ridge crests and troughs for coring. The INSS data was used to create bathymetric hillshades and digital elevation models (DEMs) of the study area, which clearly reveal a series of sinuous ridges and extensively furrowed areas of seabed (Fig. 1b). Geomorphologic characterisation of the landforms in the study area is assisted by seafloor profile analyses using the ArcGIS® 3D analyst tool.

Four vibro-cores: CE10008_42, CE10008_43, CE10008_44 and CE10008_45 (henceforth referred to as cores 42, 43, 44 and 45, respectively), were collected during the CE10008 research cruise conducted in 2010 aboard the *RV Celtic Explorer* and are used to examine the sedimentological composition of the ridges (Table 1). Information on lithology, sedimentary structures, grain size and sediment physical properties were recorded in order to reconstruct depositional environments. X-radiographs were acquired and sediment physical properties were measured prior to splitting the cores at the University of Ulster, Jordanstown and the National University of Ireland, Maynooth, respectively. Digital x-radiographs were collected using a CARESTREAM DRX Evolution system and allow improved sedimentary structure identification. X-radiograph data are displayed as sketches in the sediment logs to characterise discernible structures and display them in a usable

manner. Original, representative x-radiograph examples of lithofacies are also provided. Sediment physical properties of cores 42 and 44 were measured using a GEOTEK® multi sensor core logger and consist of P-wave velocity, wet bulk density and magnetic susceptibility. A smoothed average magnetic susceptibility value was calculated to allow comparisons between cores without anomalies caused by large clasts; this was done by removing anomalously high measurements (four measurements $>100 \text{ SI units} \times 10^{-5}$ in core 42 and three measurements $>300 \text{ SI units} \times 10^{-5}$ in core 45) from the dataset and calculating the remaining data's average. Shear stress was measured with an MCC® Impact shear vane from core centres in areas that allowed shear vane penetration without clast contact, which yields spurious measurements. Shear strength measurement intervals are typically ≤ 15 cm, except where prohibited by clast abundance. Water content is calculated as the difference between sediment wet and dry weights. Lithofacies were described visually and refined with x-radiograph examinations. Grain size analyses (GSA) were performed via laser granulometry using a MALVERN Mastersizer® at Trinity College, Dublin on 31 bulk sediment samples collected from cores at intervals guided by lithofacies data.

Table 1: sediment core information.

Core	Latitude (N)	Longitude (W)	Water depth (m)	Core length (m)
CE10008_42	53° 46.2655'	12° 38.6542'	298.5	1.76
CE10008_43	53° 43.6649'	12° 31.4036'	312.5	1.17
CE10008_44	53° 38.9150'	12° 16.8818'	295.1	2.30
CE10008_45	53° 37.7487'	12° 08.0713'	293.7	2.94

Micropaleontological analyses were conducted on 31 one-cm slab subsamples that correlate to the GSA sample intervals and are considered representative of the range of lithofacies in the cores. Benthic foraminifera assemblages were examined because they are strongly influenced by local ocean conditions (Murray, 2006). The subsamples were oven dried at $<45^{\circ}\text{C}$ for >48 hours and washed through a $63 \mu\text{m}$ sieve to remove the mud fraction. Aliquots containing >300 foraminiferal tests were divided using a Green Geological® microsplitter and dry sieved to remove the $<125 \mu\text{m}$ fraction

following the recommendation of Schönfeld et al. (2012). Foraminifera <125 µm were not counted because most foraminiferal tests below this size comprised unidentifiable fragments and recent comparative studies show that, at least for some samples, the constituents of the >63 µm fraction identify ecological controls that are similar to the >125 µm fraction (Mojtahid et al., 2009; Bouchet et al., 2012). Every identifiable foraminiferal test within the aliquots was documented to the species level whenever possible using an Olympus SZX16 low-power binocular microscope on all benthic and planktonic tests, primarily following the taxonomic descriptions of Murray (2003). Dominance (1-Simpson's index) and Fisher's α diversity statistics were calculated on benthic foraminiferal counts using the micropaleontological software PAST 3.02a (Hammer et al., 2001) on >200 tests (cf. Thomas et al., 1995; Jennings et al., 2014). Fisher's α is preferred for this study over the Shannon-Wiener index because the latter is based on relative proportions of species (Buzas and Gibson, 1969) and thus can yield spuriously high results for counts with highly dominant taxa (Dorst and Schönfeld, 2013). Fisher's α relates the count of individuals to the number of species in a sample (Fisher et al., 1943) resulting in high values indicating high diversity (e.g., Samir et al., 2003). Dominance ranges from 0.0 (all species are equally represented) to 1.0 (one species is absolutely dominant); therefore high values are associated with low diversity (e.g., Samir et al., 2003). Individual species counts are converted to relative abundances (RA), which standardises the data by describing counts as percentages of the sample population. The percentage of planktonic individuals (PTR) is calculated as a percent of the total foraminiferal count and can provide information on palaeo-surface productivity, although this must be considered strictly qualitatively in the absence of palaeo-water depths and differential dissolution data (Berger and Diester-Haass, 1988). The foraminiferal density is calculated as the ratio of the number of foraminifer individuals per mass of sediment >63 µm in milligrams (mg) and reveals qualitative, comparative information on palaeoproductivity. Severely damaged tests are defined in this study as broken or abraded beyond positive recognition of species while still comprising $\geq 50\%$ of the original material; this standard reduces the chance of over representing easily fragmented or easily recognisable (as fragments) species. Severely broken tests were counted for each sample and the severely damaged/identifiable test ratio (SDr) is calculated as a percent of the total foraminiferal count to elucidate the likelihood that foraminifera are allochthonous.

Three samples for accelerator mass spectrometer (AMS) radiocarbon analysis were selected using detailed bio-lithostratigraphic data derived from the sedimentological and micropaleontological investigations outlined above. Sediment units interpreted as ice-proximal during deglaciation on the basis of lithofacies, physical properties and foraminiferal assemblage data were specifically targeted to reveal depositional age constraints and establish a nascent retreat pattern across the Irish continental shelf. The three calcareous samples were obtained from 1 cm thick slab samples and comprise cold water coral fragments (*Lophelia pertusa*) and paired and single bivalve shells. Radiocarbon results are presented as both conventional (^{14}C BP) and corrected (Cal BP) ages (Table 4). Radiocarbon ages were calibrated using Calib© 7.0.2 software using the global ocean average Δr marine reservoir correction of 400 years because a regional marine reservoir effect is unavailable (Stuiver and Reimer, 1993).

3. Results

3.1. Geomorphology

A series of sinuous, approximately E-W trending ridges occupy the northern Porcupine Bank and Slyne Trough (Figs. 1b, 2). The ridges range from ~5 to >65 km long and are predominantly concentrated on the Porcupine Bank, with some extending continuously into the Slyne Trough (Fig. 2a, b). The two largest ridges are located in the Slyne Trough and reach heights of >30 m. The ridges are asymmetric in profile, with gentle southern and steep northern slopes (Fig. 2a, c). A broad (>5 km wide and at least 25 km long) ridge extends across the east of the study area and has a distinct NNE-SSW orientation (Fig. 2a, b). A series of high-relief (up to 15 m amplitude) corrugations oriented obliquely to the overall azimuth of the ridge occur along its crest. The southeastern corner of the study area is characterised by a gradually sloping (7.93°), relatively smooth area of seafloor. The southwestern corner of the study area is characterised by a low-relief, crenulated texture with no ridges or furrows, interpreted to be Porcupine Bank bedrock (cf. Mazzini et al., 2012).

The bathymetry also reveals long, meandering furrows that tend to cluster on the southern slopes of the ridges and in the Slyne Trough (Fig. 2a). The seafloor furrows are irregular and cross-cutting in pattern with a typical N-S orientation. They increase in size and occurrence toward the south of the study area and within the Slyne Trough where they reach depths of >10 m and are typically bordered laterally by berms (Fig. 2c). The depth of the furrows generally increases with bathymetric shallowing and often the furrows terminate on the southern slopes of the ridges in the study area (Fig. 2a).

3.2. Sedimentology

Seven lithofacies (Table 2) are identified based on core lithology, sedimentary structures and physical property measurements. These sedimentary properties are summarised in Table 2 and some of the x-radiograph facies are exemplified in Fig. 3. Three lithofacies associations are identified: lithofacies association 1 (LFA 1) is diamicton, occurs at the bottom of all four cores and consists of Dmm, Dmm_c lithofacies (Table 2; Figs. 4, 5, 6, 7); lithofacies association 2 (LFA 2) consists of Dcm and Fl lithofacies (Table 2); the tops of all four cores are represented by lithofacies association 3 (LFA 3), which consists of Sm, Sh and Suf lithofacies (Table 2; Figs. 4, 5, 6, 7).

3.2.1. Lithofacies association 1

The basal diamictons consist of Dmm lithofacies and, in cores 42 and 44, an underlying Dmm_c lithofacies (Figs. 4, 5, 6, 7), is differentiated by its high consolidation (>50-120 kPa, Table 2). In core 44, this Dmm_c diamicton is further differentiated by its low water content (<12%, Fig. 6). The diamictons are heterogeneous in colour and grain size and contain abundant >2 cm long lonestones of variable roundness. Lonestones usually consist of black, fine-grained igneous rock, but with more variable lithologies (including granite and limestone) towards the top of the diamictons. Occasional small, highly abraded shell fragments are present in the diamictons (Figs. 4, 5, 6, 7). Cores 42 and 44 consist of both Dmm and Dmm_c lithofacies; in both cores the Dmm interval is at least ~1 m thick with gradational lower contacts that separate it from the underlying Dmm_c lithofacies (Figs. 4, 6). The

diamictons of cores 42 and 43 are sandy (typical sand fractions >60%), while core 44 and 45 diamictons are muddy (sand fractions <50% and as low as 30%)(Figs. 6, 7). Shear strength measurements decrease upwards from >40 kPa to <20 kPa through the diamicton in cores 42, 43 and 44 (Figs. 4, 5, 6) and in cores 42 and 44 measurements up to 61 kPa and 123 kPa, respectively, have been recorded near the bottom of the Dmm_c lithofacies (Figs. 4, 6). The water content, wet bulk densities and P-wave velocities of these basal diamictons are typically highly variable (Figs. 4, 5, 6, 7); however, especially in core 44, the water content steadily decreases down core and reaches values as low as 11.5%. The diamicton of core 42 yields markedly lower magnetic susceptibility measurements (smoothed average measurement of 27.95 SI units x 10⁻⁵; Fig. 4) than those of core 45 (smoothed average measurement of 150.23 SI units x 10⁻⁵; Fig. 7).

3.2.2. *Lithofacies association 2*

In each core except core 43, a massive, clast-supported, ~15 cm thick Dcm diamicton with a gradational lower contact overlies the LFA 1 diamictons (Figs. 3, 6, 7). A clast supported framework is clearly identifiable in x-radiographs (Fig. 2c) and the occurrence and amount of clast contact increases upwards through the lithofacies (i.e., the amount of matrix decreases upwards); however, there is no discernible clast orientation or sorting by size. Similar to the underlying diamictons, the Dcm diamictons are heterogeneous in colour and grain size and contain abundant large (>2 cm) clasts; although, unlike lower in the cores, the Dcm clasts are composed of variable lithologies. In core 45 a ~2.5 cm long clast found 62 cm bsf (Fig. 7) exhibits distinct striations, a rounded nose and a “plucked lee” (i.e., the clast is “bullet shaped”). Sediment physical properties are also highly variable. The Dcm lithofacies contain abundant shell fragments and in core 45 the lower contact is characterised by sandy irregularities that extend sub-vertically to vertically into the underlying Dmm. The Dcm lithofacies also infrequently incorporate deformed, randomly oriented, soft-sediment clasts (Fig. 7). In core 45, the Dcm contains a soft sediment clast composed of greyish brown (2.5Y 5/2) massive mud (Fig. 7).

225 In core 43 LFA 1 is overlain by horizontally bedded sand (Sh, LFA 3) and interbedded with
 226 horizontally laminated silt and clay (Fl) (Fig. 5). The Fl lithofacies is ~5 cm thick and consists of
 227 normally graded laminations ~0.5 cm thick. The Fl interval has a sharp lower contact with the
 228 underlying Dmm diamicton. Laminae fine upwards from silty fine sand to clayey silt and have sharp
 229 lower contacts.

230 Table 2: Lithofacies summary. Codes modified from Miall (1978) and Eyles et al. (1983).

Code	Lithofacies	Description	Interpretation and [references]*
Fl	Laminated sandy silt and clay (LFA 2)	Planar, parallel laminae, ~0.5 cm thick, normally graded, with sharp lower contacts. No identified biogenic material.	Suspension settling from meltwater plumes or fine-grained turbidites; alternatively, soft sediment rip-up clasts. [1], [2], [3], [4]
Sm	Massive sand (LFA 3)	Massive, fine-to-coarse, poorly sorted sand with shell fragments; <15 cm thick; light yellowish brown (2.5Y 6/4); sharp, conformable lower contact. Coincident with apparent coring deformation.	Outer-shelf bottom-current sediment likely deformed by coring. [5], [6], [7]
Sh	Horizontally-bedded sand (LFA 3)	Poorly developed, planar, parallel beds <2 cm thick; units are 20-35 cm thick and occasionally fine upwards; typically olive (5Y 5/3); sharp or gradational lower contact. Abundant shell fragments. High water content (up to 26%). P-wave velocity from 1,000-1,800 m/s.	Outer-shelf bottom-current sediment. [5], [6], [7]
Suf	Upward-finning sand (normally graded) (LFA 3)	Massive, <40 cm thick beds of poorly sorted sand; high concentration of shell fragments, and some granules, especially low; variable colour (2.5Y 5/2 and 6/3); sharp, conformable lower contacts. Magnetic susceptibility varies from 50-200 SI units x 10 ⁻⁵ from west to east.	Outer-shelf bottom-current sediment with variable terrigenous sediment content that has been winnowed of fines. Likely records seafloor transgression. [5], [6], [7], [8], [9], [10], [11]
Dcm	Clast-supported, massive diamicton (LFA 2)	Massive, 15-20 cm thick beds of clast-supported diamicton in a sandy matrix; randomly-oriented soft-sediment clasts; shell fragments and bioturbation present; gradational lower contact. Low shear stress (<20 kPa), highest magnetic susceptibility measurements in study (up to 398 SI units x 10 ⁻⁵) and highly variable P-wave and wet bulk ρ measurements.	Glaciomarine diamicton from suspension settling with IRD and/or ice-shelf rain out. High clast concentration records increased dropstone production or winnowing of fines. Possibly reworked by iceberg turbation. [4], [12], [13], [14], [15], [16]
Dmm	Loose (<50 kPa), massive diamicton (LFA 1)	Massive, 90->200 cm thick units of unconsolidated muddy diamicton; randomly-oriented soft-sediment clasts; abundant limestones of various lithology high in core and similar lithology low; typically greyish brown (2.5Y 5/2); gradational lower contacts. Rare, small shell fragments; rare bioturbation at top. Variable P-wave and wet bulk ρ measurements.	Glaciomarine diamicton from suspension settling, IRD and/or ice-shelf rain out with areas of iceberg turbation. [12], [13], [14], [16], [17], [18]
Dmm _c	Compact (>50 kPa), massive diamicton	Massive, at least 25-80 cm thick consolidated diamicton; abundant limestones of similar lithology; variable colour (2.5Y 5/2 and 6/2); stratigraphically low with unknown lower contacts. Very rare small	Till, possibly resulting from short-lived ice shelf recoupling events that reworked and compressed existing glaciomarine sediment. Progressive

(LFA 1)	shell fragments. Low water content (typically <14%). Variable P-wave velocities and wet bulk ρ up to 2.4 g/cm ³ ; shear stress measurements up to 123 kPa.	upwards decrease in shear strength indicates a reduction in compressive vertical pressure through time. [16], [17], [19], [20], [21]
---------	--	---

* References: [1] Powell, 1983; [2] Hein and Syvitski 1992; [3] Ó Cofaigh and Dowdeswell, 2001; [4] Hillenbrand et al., 2013; [5] Bishop and Jones, 1979; [6] Fyfe et al., 1993; [7] Viana et al. 1998; [8] Robinson et al., 1995; [9] Saito et al., 1998; [10] Amorosi et al., 1999; [11] Barrie and Conway, 2002; [12] Kilfeather et al., 2011; [13] Anderson et al., 1983; [14] Eyles, 1988; [15] Vorren et al., 1983; [16] Hillenbrand et al., 2010; [17] Evans and Pudsey, 2002; [18] Smith et al., 2011; [19] Anderson, 1999; [20] Hillenbrand et al., 2005; [21] Ó Cofaigh et al., 2005.

3.2.3. *Lithofacies association 3*

The top of each core is composed of a sand interval that contains abundant shell fragments, which typically decrease in size and occurrence upwards (Figs. 4, 5, 6, 7). The sand intervals vary in structure and are categorised as Sm, Sh and Suf lithofacies (Table 2). The sand lithofacies have sharp, apparently conformable lower contacts with the underlying lithofacies and vary in thickness from 28 cm in core 43 to 50 cm in core 45. The Suf lithofacies fine upwards from poorly-sorted coarse and medium sand with granules to poorly-sorted medium sand and occur in cores 44 and 45 below Sh and Sm lithofacies with gradational lower contacts (Figs. 6 and 7). Typically, the top 5-10 cm of the sand lithofacies are deformed by the coring process.

3.3. *Micropaleontology*

Foraminifera are present in each lithofacies and analyses of all cores revealed 42 benthic taxa (Appendix 1, Tables A2, A3). Benthic foraminiferal diversity indices and general foraminiferal statistics are displayed in Appendix 1 (Table A1) and Figure 8. A maximum species richness of 24 species is counted in cores 44 and 45 at 46 cm bsf and 94 cm bsf, respectively, while the lowest count of 12 species is obtained from core 43 at 85 cm bsf. Benthic foraminiferal diversity, revealed by dominance and Fisher's α values, is highest in cores 44 and 45; in these two cores, Fisher's α values reach >0.6 and dominance values are consistently <0.2 (Fig. 8). In cores 42 and 43, diversity generally increases upwards, evidenced by dominance values that decrease upwards from >0.3 to <0.2 in both cores (Fig. 8). In all cores except core 42, foraminiferal density decreases down core from >10 to <5 tests/mg; in core 42 density is highly variable, ranging from 0.44-14.84 tests/mg with a peak at 139 cm bsf (Fig. 8).

Lithofacies association 1 generally coincides with high foraminiferal dominance (up to 0.38 in cores 42 and 43) and SDr (typically >15%) values (Fig. 8, Table 3). In cores 43, 44 and 45, LFA 1 is marked by low foraminiferal density (typically >5 tests/mg, Fig. 8). The top of LFA 1 and LFA 2 typically display a relatively abrupt increase in PTr that ranges up to 74% in core 43 (Fig. 8; Table 3). Lithofacies association 2 displays highly variable benthic foraminiferal diversity indices (Fisher's α values from 5.2-4.8 and density from 4.2-7.3; Fig. 8; Table 3). Lithofacies association 3 typically yields low values for dominance (<0.2) and SDr (as low as 8.7% in core 44), with high values (typically >10 tests/mg) for foraminiferal density (Fig. 8; Table 3).

Table 3: Lithofacies association correlations to summarised micropaleontological data.

Lithofacies association	Foraminiferal statistics	Dominant or characteristic foraminifera
1	High dominance; high SDr; low density	<i>Elphidium clavatum</i> ; <i>Cassidulina reniforme</i>
2	High PTr; variable benthic foraminifera diversity indices	<i>Discanomalina coronata</i> ; <i>Trifarina angulosa</i>
3	Low dominance; low SDr; high density	<i>Cassidulina laevigata</i> ; <i>Uvigerina mediterranea</i> ; <i>Bulimina marginata</i>

Cibicides lobatulus (Walker and Jacob, 1798) is dominant throughout the majority of the cores and common in every lithofacies (Appendix 1, Tables A2, A3). *C. lobatulus* thrives in sandy, high-current environments that experience sediment winnowing (Gooday and Hughes, 2002; Schönfeld, 2002). Despite its dominance in the population, the ubiquity of this species throughout the sediment record renders it of little use as a palaeoenvironmental proxy for this study.

Two foraminifer species associated with glacial conditions in modern oceans have been identified: *Elphidium excavatum* forma *clavatum* (Feyling-Hanssen, 1972) and *Cassidulina reniforme* (Nørvang, 1945). Both species are present throughout LFA 1, however the relative abundance of both species peaks near the top of the Dmm lithofacies (Fig. 9). The highly opportunistic species *E. clavatum* reaches relative abundances of up to 5% near the bottom of cores 44 and 45 within LFA 1 and is generally absent towards the core tops (Fig. 9). *E. clavatum* adopts both epifaunal and infaunal strategies to thrive near ice-marine interfaces with high sedimentation rates, variable salinity, average

water temperatures $<1^{\circ}\text{C}$, and often with sea ice cover (Mudie et al., 1984; Murray, 1991; Hald et al., 1993, 1994; Linke and Lutze, 1993; Hald and Korsun, 1997; Polyak et al., 2002; Stalder et al., 2014). The infaunal species *C. reniformis* is also abundant in LFA 1 (Fig. 9) and is well documented in ice-proximal marine environments in the northeastern Atlantic (Sejrup and Guilbault, 1980; Hald and Korsun, 1997; Sejrup et al., 2004). These species are typically well preserved in LFA 1, displaying less breakage and abrasion than many of the accompanying foraminifer species.

In most cores, the relative abundances of *Discanomalina coronata* (Parker and Jones, 1865) increase just below the lower contact of LFA 2 (Fig. 9). *D. coronata* is common in areas with high bottom currents and coarse sediment or bedrock (Hald and Vorren, 1987; Schönfeld, 1997) and is reported to thrive in areas of dead coral fragments (Morigi et al., 2012; Smeulders et al., 2014). *D. coronata* is associated with areas of bedrock that are distal to coral mounds on the modern Porcupine Bank (Smeulders et al., 2014). The infaunal foraminifer species *Trifarina angulosa* (Williamson, 1858) is abundant throughout the examined cores and has been documented as a common species on the Porcupine Bank (Weston, 1985; Smeulders et al., 2014) and in Atlantic polar front regions (Mackensen et al., 1993). *T. angulosa* is reported to thrive in areas of coarse sediment and high bottom currents (Mackensen et al., 1993; Klitgaard Kristensen and Sejrup, 1996) and in cores 42 and 43 its relative abundances undergo rapid changes near the lower contact of LFA 2 (Fig. 9). *Cibicides refulgens* (de Montfort, 1808) is also common near LFA 2 and is associated with high bottom currents and areas of sediment winnowing (Goody and Hughes, 2002; Smeulders et al., 2014).

The dominant foraminifer species in LFA 3 are the epifaunal *Cassidulina laevigata* (d'Orbigny, 1826, 1847) and infaunal species *Uvigerina mediterranea* (Hofker, 1930) (Fig. 9). Both species are associated locally with sheltered areas, preferentially on or near cold-water coral mounds (Smeulders et al., 2014). *Bulimina marginata* (d'Orbigny, 1826) is common near the core tops and is also associated with modern living and dead coral mounds on the Porcupine Bank (Morigi et al., 2012; Smeulders et al., 2014) as well as phytodetrital sediment in the Rockall Trough (Goody and Hughes, 2002).

3.4. Chronology

AMS radiocarbon dating was conducted on three samples consisting of bivalve shells and cold-water coral (*Lophelia pertusa*) fragments; results are summarised in Table 4. The radiocarbon ages are within marine isotope stage (MIS) 2. The oldest radiocarbon age recovered in this study is ~25 Cal. kaBP. This age is derived from a *Lophelia pertusa* fragment collected 180 cm bsf in core 44, encased in a Dmm_c diamicton (Fig. 6). *Lophelia pertusa* is known to colonise the modern seafloor near the study area (Scoffin and Bowes, 1988; Heindel et al., 2010; Smeulders et al., 2014) and thus is considered a viable source of locally bio-mineralised radiocarbon-datable material. The youngest age of ~19ka Cal. BP is from a paired, unabraded and unbroken bivalve shell; this sample was collected from Suf sand (the only age derived from a non-diamictic lithofacies) 36 cm bsf in core 42 (Fig. 4; Table 4). A single (unpaired), unbroken and unabraded bivalve shell sampled from Dmm diamicton 94 cm bsf in core 45 yielded an age of ~20 ka Cal. BP (Table 4). All specimens sampled for radiocarbon dating were largely free of obvious surface wear and are deemed to have been incorporated into the surrounding sediment close to their point of origin based on the quality of their preservation.

Table 4: radiocarbon results.

Core	Depth (cm bsf)	Sample material	¹⁴ C age (yrs. BP)	Calibrated age (yrs. BP)	δ ¹³ C (‰)	Surrounding lithofacies	Laboratory code
42	36	Paired bivalve shell	17900±89	19182±155	-4.7	Suf	Poz-66484
44	180	Coral fragment	20710±90	24720±260	-1.3	Dmm _c	Beta-334419
45	94	Single bivalve shell	18733±107	20254±151	4.3	Dmm	Poz#2-66430

4. Interpretation

4.1. Geomorphology

4.1.1. Seafloor furrows

Seafloor furrows are common in the study area and are concentrated in the Slyne Trough (Fig. 2). Because of their irregular patterns, adjacent presence of lateral berms (Fig. 2a) and bathymetric association (amplified depth and berm formation with height), the seafloor furrows are interpreted as iceberg scours (Belderson et al., 1973; Dowdeswell et al., 1993; Ó Cofaigh et al., 2002, 2010); the common N-S orientation and tendency to deepen or end on the southern ridge slopes suggest a calving ice margin toward the south of the study area and a northward palaeocurrent direction. Thus we interpret the primary ice source to be the BIIS, which is in agreement with an ice-rafted detritus (IRD) study of deep sea cores along the western BIIS continental margin (Scourse et al., 2009).

4.1.2. Seafloor ridges

Sinuuous ridge asymmetry is typical of the ice proximal/distal discrepancy expected from glacial push moraines (Boulton, 1986). Some ridges possess southern slopes with low gradients (Fig. 2b), forming an asymmetrical profile that more closely resembles grounding-zone wedges (e.g., Bart and Cone, 2012; Dowdeswell and Fugelli, 2012; Jakobsson et al., 2012). However, the sinuosity and in places “scalloped” form of the ridges contrasts slightly with typical, arcuate end moraine structures (e.g. Bradwell et al., 2008; Ó Cofaigh et al., 2010).

Although the geomorphic interpretation of the individual E-W trending ridges is uncertain, the parallel to sub-parallel, ostensibly sequential organisation of the ridges across the study area, coupled with their extension across varied terrain suggest ice-marginal formation. Furthermore, the intensive iceberg scouring supports the concept of a nearby palaeo-ice margin. Thus, the landforms are tentatively interpreted as a record of westward BIIS extension across the Irish continental shelf. Due to discrepancies in scale and morphology with previously documented BIIS end moraines west of Ireland (which are arcuate and reach lengths of ~125 km; Ó Cofaigh et al., 2010; Clark et al., 2012a) an interpretation of ice-marginal deposition during relatively short-lived ice extensions with an actively calving margin is preferred. The radiocarbon ages recovered from on and near the sinuous ridges date from MIS 2, demonstrating that the landforms incorporate calcareous material that was bio-mineralised during the Midlandian Glaciation.

The orientation of the large, corrugated SSW-NNE trending ridge relative to the aforementioned abundant E-W trending ridges suggests a different geomorphic evolution. The corrugations are apparently a series of E-W trending ridges that are overprinted on the larger SSW-NNE trending ridge. They have a similar orientation to the neighbouring sinuous ridges and appear to be situated as eastward extensions of those ridges (Fig. 2a). Because of these characteristics, we tentatively interpret this ridge as an earlier glacial landform, likely an end moraine, which has been subsequently overprinted by the E-W trending ridges.

4.2. Sedimentology and palaeoenvironment

The four cores analysed for this study are interpreted to provide a record of glacial glacial sedimentation in the Slyne Trough and on the Porcupine Bank. Two of the cores (44 and 45) are taken from near the crests of moraines in the Slyne Trough and recover 2.3-2.9 m of sediment. Because this sediment has properties characteristic of subglacial deposition and is sampled from the moraine crests, we interpret it as the ridge-forming deposit.

4.2.1. Lithofacies association 1

The massive structure, low water content and high (50-123 kPa) shear strength that characterise the Dmm_c lithofacies are consistent with vertical compaction from an overriding glacier; the progressive up-core decrease in shear strength suggests a gradual decrease in compaction over time (Anderson, 1999; Evans et al., 2005). Furthermore, the striated, “bullet shaped” morphologic characteristics on a clast sampled from core 45 are interpreted to indicate proximal subglacial transport (Sharp, 1982). The presence of heavily fragmented shell material indicates that the diamicton incorporated earlier marine deposits and the westward decrease in magnetic susceptibility measurements denotes a reduction in terrigenous sediment supply (Robinson et al., 1995; Shevenell et al., 1996). These variables are interpreted as a record of subglacial sedimentation (till, Fig. 10). The incorporation of biogenic material and reduction of magnetic susceptibility along the geographically and geomorphologically interpreted ice flow direction (westward) suggests either a subglacial

sediment supply that incorporated large amounts of pre-glacial marine sediment or an ice mass that was only periodically grounded and failed to transport large amounts of terrigenous sediment to the shelf edge (cf. Ó Cofaigh et al., 2005; Garcia et al., 2011).

The Dmm lithofacies are characterised by abundant lonestones in a less compact (shear strength <50 kPa, often <10 kPa), mud-rich matrix that is consistent with subglacial deposition as a dilatant till (Evans et al. 2005; Ó Cofaigh et al., 2005, 2007), or glaciomarine sedimentation from suspension settling and IRD (Evans and Pudsey, 2002; Hillenbrand et al., 2005; Kilfeather et al., 2011; Smith et al., 2011). The relative paucity of observable shell fragments or bioturbation in the Dmm diamicton from cores 42 and 44 and the bottom of core 43 (Figs. 4, 5, 6), along with their variable and moderate shear strengths (8-42 kPa) suggests that these diamictons are a dilatant till deposited over a highly compact till unit by a deforming, overriding ice mass (e.g. Smith, 1997; Vaughan et al., 2003; Ó Cofaigh et al., 2005). Conversely, the low shear strength (<15 kPa), relatively abundant shell fragments, appearance of till pellets and bioturbation within the Dmm diamicton of core 45 and at the top of LFA 1 in core 43 (Figs. 5, 7) suggest that the diamicton was deposited by proglacial or sub-ice shelf rainout (e.g., Evans and Pudsey, 2002; Hillenbrand et al., 2005; Kilfeather et al., 2011; Smith et al., 2011). The stratigraphic position of the proglacial suspension sediment above the dilatant till in core 43 indicates that the suspension settling occurred during BIIS retreat from the Porcupine Bank.

Lonestones within the sub-ice shelf or proglacial Dmm diamicton are interpreted as IRD based on their random orientations and variable sizes (e.g., Grobe, 1987; Heinrich, 1988). Their abundance suggests intense iceberg activity or periods of sub-ice shelf sedimentation (Evans and Pudsey, 2002). A sub-ice shelf interpretation is supported by the lithologic similarity of the dropstones at the base of the Dmm diamicton, which tends to be variable in open-water environments (Pudsey and Evans, 2001; Domack et al., 2005). Thus, the Dmm diamicton in core 45 and at the top of LFA 1 in core 43 is interpreted as *in situ* sub-ice shelf or ice-proximal iceberg rain-out sediment (Fig. 10).

High foraminiferal dominance values and the commonly low foraminiferal density in LFA 1 (Table 3) suggest poor palaeoproductivity. The typically low PTr values of LFA 1 may indicate a reduction in surface productivity (Diester-Haass, 1978; Ovsepyan et al., 2013), although this metric may also reflect changes in sea level and rates of carbonate dissolution (Berger and Diester-Haass, 1988). An anomalously low PTr value of 21.5% is recorded in core 42 at 78 cm bsf (Fig. 8), which correlates with the highest SDr value (35.8%) recorded in this study; this suggests that the low PTr value may record the preferential breaking of fragile planktonic tests during sediment reworking or sample processing rather than actual palaeoenvironmental conditions. The occurrence of well-preserved *E. clavatum* and *C. reniforme* near the top of LFA 1 suggests a palaeoenvironment that experienced high sedimentation rates, variable salinity and average water temperatures $<1^{\circ}\text{C}$ (Murray, 1991; Hald et al., 1993, 1994; Linke and Lutze, 1993; Hald and Korsun, 1997; Sejrup et al., 2004). The Dmm_c lithofacies at the bottom of core 44 is associated with a high SDr value ($>25\%$; Fig. 9), which suggests an increased amount of subglacial and ice-proximal transport in this sediment (Melis and Salvi, 2009). Because of its sedimentological and micropaleontological characteristics, LFA 1 is interpreted to indicate glacial conditions that likely experienced ice-proximal meltwater influx, cold temperatures and periods of overriding by the BIIS that resulted in sediment compaction (Dmm_c) and the incorporation of allochthonous foraminifer species.

Two AMS radiocarbon dates are derived from samples taken from LFA 1 between 75 and 180 cm bsf (Fig. 10; Table 4). These dates range from $24,720 \pm 260$ to $20,254 \pm 151$ Cal. BP, confirming a Midlandian depositional age. The ages are from cores 44 (180 cm bsf) and 45 (94 cm bsf) and constrain the deposition of the Dmm_c and overlying Dmm lithofacies, respectively (Fig. 10; Table 4). In core 44 the date from 180 cm bsf provides a maximum age for the diamicton and indicates that its deposition occurred after $24,720 \pm 260$ Cal. BP (Fig. 10). In core 45 the sample from 94 cm bsf also provides a maximum age for the Dmm diamicton and indicates that it was deposited after $20,254 \pm 151$ Cal. BP (Fig. 10).

4.2.2. Lithofacies association 2

The similarities in clast size, roundness and lithology between the Dcm lithofacies and the top of the underlying LFA 1 diamictons suggest a similar primary sediment source. Thus the increase in clast contact in LFA 2 is interpreted as the result of either fine sediment winnowing (Eyles, 1988) or a period of increased IRD production (Kilfeather et al., 2011). Fine sediment winnowing may result from increased palaeocurrents. Given the geomorphically interpreted, northward palaeocurrent direction through the Slyne Trough, it is plausible that palaeocurrents may have been hindered by ice occupation and, thus, ice loss would have resulted in an abrupt palaeocurrent increase. An increase in IRD production may also result from ice shelf break up (Kilfeather et al., 2011). Soft-sediment clast inclusions have similar sedimentary properties to the underlying diamicton and are interpreted as rip-up clasts that were likely dislodged during iceberg turbation (Hillenbrand et al., 2013) or till pellets from iceberg rainout (Ovenshine, 1970). The IRD lithological variability indicates a multitude of sediment provinces, which suggests the establishment of an open-water environment and deposition from icebergs (Domack et al., 2005). The vertical, sandy irregularities that bisect the lower contact of the Dcm diamicton in core 45 are interpreted as infilled burrows (bioturbation, Fig. 7); this and the increased occurrence and size of shell fragments support an interpretation of deposition during ice shelf break up leading to an open water environment and an increasingly distal ice margin (Smith et al., 2011).

Based on its planar, parallel structure and silty fine sand to clayey silt texture, the Fl lithofacies may be interpreted as ice-distal suspension sediment or a fine-grained turbidite. Its position within the IRD-rich glaciomarine diamicton (Dmm) and its discrete occurrence in the core suggest that it is most likely a turbidite that originated on the nearby 1.4° slope of the Porcupine Bank or the flanks of sediment ridges (Fig. 2). This interpretation is supported by previous studies that document subaqueous fine-grained turbidite formation on similar gradient slopes (e.g., Schwab et al., 1996). Alternatively, the Fl lithofacies may be a large soft-sediment clast that happens be oriented with its laminae horizontal and spans the 11 cm width of the core. If this interpretation is correct, the Dmm lithofacies in core 43 is relatively rich in rip-up clasts (cf. Hillenbrand et al., 2013) and their similarity to the underlying Dmm diamicton suggests that they are plucked from overridden glaciomarine

deposits and subsequently deposited below a floating ice mass as till pellets (Domack et al. 1999; Evans et al. 2005; O Cofaigh et al. 2005). Either interpretation is compatible with sedimentation during transition from ice-proximal glacial conditions to the establishment of open-water conditions following an eastward retreating ice margin.

The abrupt increase in PTr values in LFA 2 indicates an increase in surface productivity (Diester-Haass, 1978; Ovsepyan et al., 2013), which supports an interpretation of ice break up and retreat. Lithofacies association 2 also marks the transition to a palaeoenvironment dominated by foraminifer species associated with modern, high-current conditions on the Porcupine Bank. The increase in *D. coronata* relative abundance just below the lower contact of LFA 2 suggests an increase in palaeocurrent velocities (Hald and Vorren, 1987; Schönfeld, 1997). Increases in the relative abundance of *C. refulgens* also indicates energetic palaeocurrents and sediment winnowing (Gooday and Hughes, 2002; Smeulders et al., 2014). Rapid, although occasionally opposing, fluctuations in the relative abundance of *T. angulosa* suggest a period of palaeoenvironmental transition. Because of these foraminiferal characteristics this group is considered indicative of a transition to unsheltered habitats that experience high currents and receive a relatively high food supply.

Based on its sedimentological and micropaleontological characteristics, LFA 2 is interpreted to record a transitional period between the underlying ice-proximal and subglacial sediment and the overlying sandy deposits of LFA 3. This transitional period likely experienced an increase in palaeocurrent activity that coincided with an increased rate of IRD sedimentation. These conditions likely resulted from an increase in the geomorphically-revealed northward palaeocurrent due to the loss of an ice mass over or grounded to the Slyne Trough. Additionally, ice shelf break up in the area could also account for an increase in IRD production. These conditions are interpreted to mark the initiation of BIIS retreat and the establishment of open ocean conditions in the area. The age of these lithofacies is constrained by AMS radiocarbon dates derived from underlying and overlying strata to between $20,254 \pm 151$ and $19,182 \pm 155$ Cal. BP (Fig. 10).

4.2.3. Lithofacies association 3

Based on lithology, structure, biogenic content, stratigraphic position and geographic position on the shelf, LFA 3 is interpreted as postglacially-reworked glacigenic material (cf. Fyfe et al., 1993). A glacially-influenced, primary depositional environment is supported by the higher magnetic susceptibility measurements in core 45 (smoothed average SI units $\times 10^{-5}$ of 150.23, Fig. 7) relative to the westernmost core 42 (smoothed average SI units $\times 10^{-5}$ of 27.95, Fig. 4), which may indicate higher terrigenous sediment supplies to the east (Robinson et al., 1995; Shevenell et al., 1996). The sands were likely reworked by strong, but gradually weakening (suggested by Suf lithofacies), bottom currents (Bishop and Jones, 1979; Fyfe et al., 1993; Viana et al. 1998). This interpretation is further supported by winnowing in the underlying LFA 2 and previous micropaleontological (Smeulders et al., 2014) and sedimentological (De Haas et al., 2009) studies on the Porcupine Bank and flanks of the nearby Rockall Trough. This gradual palaeocurrent weakening is interpreted as a signature of sea level transgression on the Irish continental shelf and shares similar sedimentary characteristics with other postglacial transgressive marine sediment deposits and stratigraphic sequences (Saito et al., 1998; Amorosi et al., 1999; Barrie and Conway, 2002).

The low foraminiferal dominance values in LFA 3 (Fig. 8; Table 3), indicate high surface palaeoproductivity (Diester-Haass, 1978; Ovsepyan et al., 2013). The typically high foraminiferal density values also indicate increased palaeoproductivity, likely from decreasing glacial influence (Hebbeln and Wefer, 1991; Carmack and Wassmann, 2006). The increasing relative abundance of *C. laevigata*, *U. mediterranea* and *B. marginata* in LFA 3 suggests an increased food supply and the emergence of a palaeoenvironment resembling modern “on-mound” (i.e. on cold water coral mounds) environments on the Porcupine Bank (Smeulders et al., 2014). Thus, based on its sedimentological and micropaleontological attributes, LFA 3 is interpreted as outer-shelf bottom-current sediment with variable terrigenous sediment content that has been winnowed of fines; the normal grading of the Suf lithofacies records sea level transgression (Bishop and Jones, 1979; Fyfe et al., 1993; Viana et al. 1998).

The age of LFA 3 is constrained by an AMS radiocarbon age derived from 36 cm bsf in core 42 to likely be younger than 19182 ± 155 Cal. BP (Fig. 10; Table 5). Because this age is calculated from the westernmost (likely most ice-distal) core, it is interpreted to most accurately represent the earliest phase of post-glacial sedimentation in the study area. This record of transgression is slightly earlier than some terrestrial (shoreline) data indicators (e.g., Kuchar et al., 2012), which is likely the result of an earlier onset of deglaciation and a diminished glacio-isostatic effect on the outer shelf.

5. Discussion

5.1. The late Midlandian BIIS on the Porcupine Bank

5.1.1. Signature of BIIS position

The seafloor morphology of the study area is dominated by long, sinuous ridges seemingly deposited sequentially across the northern flank of the Porcupine Bank and the Slyne Trough (Figs. 2, 11a). These ridges are largely composed of glaciomarine diamicton (LFA 1) that tends to be compact (>50 kPa) and low in water content towards the core bottoms, suggesting periods of BIIS overriding and compression (Anderson, 1999; Evans et al., 2005). Homogeneous clast lithology and structure in the lower diamicton (Dmm_c and upper Dmm) suggests a subglacial or sub-ice shelf origin (Pudsey and Evans, 2001; Domack et al., 2005). Changes in LFA 1 magnetic susceptibility (Figs. 4, 7) and grain size (sand-sized particles 30% by weight in core 45 Dmm and 69% in core 43 Dmm) across the study area suggest that the BIIS overrode and remobilised pre-glacial material as till (cf. Evans and Ó Cofaigh, 2003; Ó Cofaigh et al., 2011). The abundance of foraminiferal tests (up to 1.3-1.4 benthic individuals/mg in core 44, Appendix 1, Table A3) with signs of remobilisation (SDr up to 25% in core 44, Fig. 8) and the presence of both cold and warm water taxa in the Dmm_c lithofacies supports an interpretation of glactectonised pro- and pre-glacial marine material (Hald et al., 1990; Melis and Salvi, 2009). Thus, the ridges are interpreted as a combination of BIIS end moraines, grounding-zone wedges, or possibly push ridges from ice shelf recoupling (Fig. 11). An interpretation of ridge formation from temporary ice shelf recoupling is compatible with sedimentary and

micropaleontological evidence of ice shelf formation. Furthermore, the sequential ridge formation is concentrated on bathymetric highs on the Porcupine Bank and Slyne Trough, suggesting formation along a floating ice mass during periods of grounding (Fig. 2).

The large, corrugated ridge in the east of the study area is geomorphically and, presumably, genetically distinct from the abundant sinuous ridges. Individual corrugations appear to be oriented with the smaller moraines on the Porcupine Bank and Slyne Trough (i.e. as extensions thereof) and have a similar scale (Fig. 2). This suggests that the corrugated ridge is overprinted by the smaller, sinuous ridges and is therefore older. Based on its differing orientation, larger scale, and apparent older age, we hypothesise that this large ridge is a BIIS terminal moraine (or grounding-zone wedge) deposited in front of an ice lobe that was grounded to the continental shelf. In the absence of any chronological control, it is unknown if this landform dates to the Midlandian or an earlier glaciation.

5.1.2. Ice shelf formation and break up

The Dmm diamicton in core 45 and overlying the dilatant till at the base of core 43 is interpreted to record a period of post-grounded ice advance, sub-ice shelf sedimentation based on its loose consolidation (typically <15 kPa), abundant dropstones, incorporation of till pellets, and upwards increase in biogenic activity (bioturbation and shell fragments) (cf. Hillenbrand et al., 2010; Kilfeather et al., 2011). The presence of till pellets and abundant dropstones oriented randomly within a matrix of fine-grained sand and mud is consistent with sedimentation from rain out from icebergs or ice shelves (Evans and Pudsey, 2002; Hillenbrand et al., 2005; Kilfeather et al., 2011; Smith et al., 2011). Clast lithologic homogeneity is similar between the lower glaciomarine sediment and the underlying till, suggesting a sub-ice shelf depositional environment (Pudsey and Evans, 2001; Domack et al., 2005; Kilfeather et al., 2011) or a proximal ice source. The formation of an ice shelf is supported by the common, upwards increases in planktonic foraminifera and overall foraminiferal densities in the Dmm diamicton (Fig. 8) because these increases suggest an increase in palaeoproductivity (Hebbeln and Wefer, 1991; Carmack and Wassmann, 2006), which may have resulted from the introduction of relatively warm Atlantic water influx (cf. Kilfeather et al., 2011; Fig.

11). The successive, sinuous ridges along the Porcupine Bank and Slyne Trough are also compatible with the development of an ice shelf following the advance of grounded ice across the shelf to the Porcupine Bank. This ice shelf likely developed over the Slyne Trough, with the Porcupine Bank acting as a pinning point (e.g. Joughin et al., 2004) during initial uncoupling (Fig. 11).

An upwards increase in lithological heterogeneity through the glaciomarine (Dmm) diamicton suggests the emergence of a period of IRD deposition from ice with multiple source areas (Pudsey and Evans, 2001; Domack et al., 2005). We interpret this as the signature of initial ice shelf break up that lead to the eventual establishment of open water conditions (cf. Kilfeather et al., 2011). A period of either increased palaeocurrent activity that enabled winnowing, or increased coarse sediment supply, or a combination of both followed the ice break up, evidenced by the Dcm lithofacies that overlies the glacial diamicton (Fig. 11).

The numerous iceberg scours in the study area appear preferentially aligned with the Slyne Trough and indicate a roughly N-S oriented palaeocurrent following the ice shelf break (Figs. 2a, 11d). Further qualitative geomorphic evidence for an approximately northward palaeocurrent is provided by a common northward deepening of scours against the rising floor of the Slyne Trough and scours that terminate on the southern flanks of ridges (Figs. 2a, 11d). If this palaeocurrent interpretation is correct, the extension of the ice sheet over the Slyne Trough may have sufficiently disrupted local palaeocurrents through the Slyne Trough to allow the deposition of silt and clay seen in the underlying Dmm_c and Dmm lithofacies (Fig. 11).

5.2. Implications for BIIS chronology

5.2.1. BIIS extent and chronology of advance

We present multiproxy data on ice position that indicates a ~80 km extension from previous reconstructions of maximum BIIS extent west of Ireland that locate the maximum extent approximately along the Galway Lobe Moraine (Sejrup et al., 2005; Scourse et al., 2009; Clark et al., 2012a; Fig. 1a). This ice advanced as a grounded ice mass that traversed the Slyne Trough to the

northern Porcupine Bank (Figs. 1, 11). This extension constitutes a ~180 km advance offshore of County Mayo, Ireland at maximum extent. This places BIIS maximum extent ~100-km farther west from the shelf moraines offshore of County Donegal described by Benetti et al. (2010), Ó Cofaigh et al. (2010) and Dunlop et al. (2010) and provides supporting evidence for grounded ice extension to the shelf edge west and north of Ireland. The new extent adds a ~6,700 km² areal increase over previous BIIS estimates, summarised by Clark et al. (2012a) to be ~840,000 km². This constitutes a ~3% increase in the estimated areal extent of the BIIS Irish Sector, previously projected to have reached ~222,500 km² (Greenwood and Clark, 2009). Sedimentary and micropaleontological evidence indicates that this ice mass likely uncoupled from the seafloor and formed an ice shelf prior to retreat (Fig. 11).

Three new AMS radiocarbon ages are the first to constrain the advance of the BIIS onto the western Irish continental shelf to within the last $24,720 \pm 260$ Cal. BP (Table 5; Figs. 10, 11a). The oldest date of $24,720 \pm 260$ Cal. BP (Table 5) is sampled from a Dmm_c diamicton interpreted to be till based on its high consolidation (>80 kPa) and low water content (<14%) (Fig. 6). This suggests an ice advance at least as far offshore as the Slyne Trough $\leq 24,720 \pm 260$ Cal. BP; this is $\geq 2,000$ years younger than previous estimates of BIIS extension to the western Irish shelf edge established by radiocarbon ages from IRD-rich sediment along the western Irish margin and Rosemary Bank (Peck et al., 2006; Scourse et al., 2009) and sediment supply to the Donegal-Berra Fan (Wilson et al., 2002). However, this younger advance is consistent with a scenario of continued BIIS extension beyond the previously suspected last glacial (Midlandian) maximum extent on the Irish continental shelf (Fig. 1a). Midlandian ice advance to the Slyne Trough suggests that the shelf moraines west and north of County Donegal (Benetti et al., 2010; Dunlop et al., 2010; Ó Cofaigh et al., 2010) were also likely deposited during the last glaciation. This ice sheet advance towards the Porcupine Bank likely predates formation of the large Galway Lobe Moraine on the shelf west of Ireland (Clark et al., 2012a; Fig. 1). This is consistent with the interpretation of the large corrugated ridge (Fig. 2a, b) as an earlier, potentially Midlandian, BIIS moraine and previous geomorphological models of Irish Ice Sheet behaviour (e.g., Greenwood and Clark, 2009; Clark et al., 2012a).

5.2.2. Chronology of BIIS retreat

The importance of establishing a complete record of BIIS retreat is outlined by Clark et al. (2012a) and improvements should logically begin with refining ice sheet chronology and maximum extent. This paper provides the geographic and chronologic starting points for retreat rate calculations for the westernmost margin of the BIIS. AnAMS radiocarbon age of $19,182 \pm 155$ Cal. BP (Table 5) derived from postglacial lithofacies (LFA 3) that overlie the transitional glaciomarine lithofacies (LFA 2) dates the establishment of open water conditions (Fig. 11c, d). This age confines the likely duration of BIIS occupation on the outer shelf as either grounded or floating ice to a ~5,500 year window commencing ~25,000BP and with retreat underway by ~19,500 BP (Fig. 11). Ice occupation may have been prolonged by the development of an ice shelf that acted as a buttress against ice flow (Rignot et al., 2004; Alley et al., 2007; Fig. 11).

Given this chronologic evidence, we interpret the Galway Lobe Moraine as a recessional moraine or grounding-zone wedge. The Galway Lobe Moraine's flat-topped morphology (Clark et al., 2012a; Fig. 1b) is compatible with formation as a grounding-zone wedge (cf. Bart and Cone, 2012; Dowdeswell and Fugelli, 2012; Jakobsson et al., 2012) and its large size (>20 km wide, Fig 1b) suggests that it was formed during a significant stillstand during retreat (Dowdeswell et al., 2008). This stillstand may be the product of ice flow buttressing by the ice shelf that persisted over the Slyne Trough, which is evidenced by sub-ice shelf sedimentation and paleontological indications for ice-proximal meltwater influx and cold temperatures.

No other age constraints are currently available across the western Irish shelf. Thus we are forced to consider terrestrial age constraints from the west of Ireland to assess implications for marine termini retreat rates. Many terrestrial ages from the west of Ireland are contested (e.g., Bowen et al., 2002; Ó Cofaigh and Evans, 2007; Clark et al., 2009, 2012a; Ballantyne, 2010) and relatively few are available from counties Galway and Mayo (Clark et al., 2012a). Most ages place initial deglaciation of the west Irish coast around ~20 kyr BP (McCabe et al., 2005; Ballantyne, 2010; Clark et al., 2012a). Thus, we agree with the assessment of Ballantyne (2010) that the best estimate for the start of

terrestrial deglaciation (ice free “peripheral zones”) is ~20 ka BP. This estimate suggests that retreat for the ~180 km long western BIIS marine sector occurred during a ~1,000-2,500 year time window, yielding a range of possible retreat rates from ~180 to 72 myr⁻¹. These rates are comparable to those for BIIS retreat along the Irish Sea Lobe marine-terminating margin, estimated at 145 myr⁻¹ (Clark et al., 2012). Other comparable estimates for retreat rates are reported from Antarctic marine margins during West Antarctic Ice Sheet retreat from the outer Antarctic Continental Shelf during the last deglaciation in the Ross and Bellingshausen seas (Conway et al., 1999; Kilfeather et al., 2011).

6. Conclusions

- Geomorphic, sedimentary and micropaleontological data from the Porcupine Bank and Slyne Trough, west of Ireland, indicate that a series of sinuous ridges on the outer shelf are most likely moraines or grounding-zone wedges. Their presence confirms and extends the geomorphological evidence of BIIS extension across the Irish continental shelf.
- These new data extend the BIIS margin by up to ~80 km further to the west. This equates to an estimated 6,700 km² areal increase in grounded ice and a ~3% increase in the estimated areal extent of the BIIS Irish Sector.
- A radiocarbon age sampled from highly consolidated till that underlies loose dilatant till provides the first constraints on the timing of BIIS marine margin advance to after 24,720±260 Cal. BP.
- Ice shelf development and possible readvance(s) onto the Porcupine Bank likely followed uncoupling of the grounded ice sheet on the Slyne Trough. The northern Porcupine Bank probably acted as an ice shelf pinning point during uncoupling and minor readvances are recorded by glaciogenic ridges.
- Sedimentological and micropaleontological evidence are strongly stratigraphically correlated and record ice shelf break up and the establishment of open water conditions over the Slyne Trough.

- A radiocarbon age from the draping Holocene marine sediment constrains ice shelf break up to before $19,182 \pm 155$ Cal. BP, following a $\leq 5,500$ year occupation and a retreat rate of ~ 180 to 72 myr^{-1} from the northern Porcupine Bank to the Slyne Trough.
- Iceberg scours indicate a roughly northward iceberg trajectory following ice shelf break up. Icebergs were concentrated in the Slyne Trough where palaeocurrents forced iceberg keels into bathymetric highs, suggesting a BIIS ice provenance.

7. Acknowledgements

JLP acknowledges a University of Ulster PhD studentship and Vice-Chancellor's Scholarship from 2013-2016. Funding for AMS radiocarbon dates was provided by the UK Natural Environment Research Council (NERC) BRITICE-CHRONO consortium grant: NE/J009768/1, the International Association of Sedimentologists (Postgraduate Research Grant, 1st session, 2014) and the Raidió Teilifís Éireann (RTE) broadcasting company for the television programme 'The Investigators'. We acknowledge data-acquisition support from the Integrated Mapping for the Sustainable Development of Ireland's Marine Resources (INFOMAR) program and Christian Wilson of Ocean DTM for geotiffs of OLEX data. Grateful thanks go to Robin Edwards at Trinity College, Dublin for the use of his MALVERN Mastersizer[®] for grain size analyses and sample processing and Stephen McCarron at the National University of Ireland, Maynooth for the use of his GEOTEK multi-sensor core logger. SB would like to thank the Captain and Crew, of RV Celtic Explorer, PI Aggie Georgiopoulou (UCD), cruise participants and Mr Áodhan Fitzgerald of the Marine Institute, for their invaluable assistance during cruise CE10008. This research survey was carried out under the Sea Change strategy with the support of the Marine Institute and the Marine Research Sub-programme of the National Development Plan 2007–2013. We acknowledge the constructive input provided during review of this manuscript by David Peter Vaughan-Hirsch and an anonymous reviewer.

Figure captions

Figure 1: **(a)** Regional schematic map locating the study area (bold black rectangle) amongst BIIS extents (discussed in text) and relevant palaeoglaciological features west of Ireland. Core locations shown as white dots. “Previous westernmost BIIS extent” represents BIIS extent prior to this study and is modified from Sejrup et al. (2005), Scourse et al. (2009), Clark et al. (2012a) and Sacchetti et al. (2012); “BIIS maximum (this study)” incorporates interpretations from this study. The “Previously accepted LGM” is adapted from Bowen et al. (1986). Abbreviations: D.B. = Donegal Bay, G.B. = Galway Bay. **(b)** DEM of the study area created from an INFOMAR bathymetric raster; area coincides with the bold black rectangle in (a). Core locations are shown as labelled white dots. Arrows 1 and 2 indicate sinuous ridges and arrow 3 marks the large, corrugated N-S trending ridge. The large moraine mapped by Clark et al. (2012a) is visible and labelled (referred to here as the Galway Lobe Moraine) in the hillshaded OLEX® data west of the study area (Courtesy of Ocean DTM).

Figure 2: **(a)** INFOMAR bathymetric 25-m resolution DEM revealing seafloor morphology and core locations (white, labelled dots). Sets of sinuous, E-W trending ridges are discernible and some are highlighted with grey dashed lines. The large, corrugated, roughly N-S trending ridge is outlined with a black dashed line; individual corrugations are indicated with arrows. Seafloor furrows are visibly concentrated within the Slyne Trough and towards the south of the study area. A series of approximately N-S oriented transects (X-X', Y-Y', Z-Z') correlate to seafloor profiles shown in (c); a small (0.6 km long) transect labelled FP (Furrow profile) bisects a prominent, but fairly typical, seafloor furrow and correlates with the ‘Furrow profile’ in (c). **(b)** Geomorphic map depicting the geographical locations of the sinuous ridges, corrugated ridge and core locations on the Porcupine Bank and Slyne Trough. Transect A-A' corresponds with the sedimentary profile provided in the interpretation section. **(c)** Seafloor profiles derived from transects in (a). Profile X-X' is >18 km long and bisects three prominent sinuous ridges (red arrows) and possibly two subtle ridges (blue dotted arrows) to the north and south of core 43. Y-Y' and Z-Z' bisect large ridges within the Slyne Trough near cores 44 and 45, respectively; both elucidate areas of intense furrowing on the southern flanks of the ridges. Furrows on the southern flanks of ridges are visible on all three profiles. The furrow profile reveals a depth of ~10 m and flanking berms >3 m high.

Figure 3: Representative x-radiograph facies. **(a)** Horizontally-bedded sand in Core 45; black arrows highlight some of the prominent horizontal structures. The unit also fines upwards and has less biogenic material at its top. **(b)** Upward fining sand with areas of bioturbation (prominent burrows outlined with white dotted lines) in Core 42. **(c)** Massive, clast-supported diamicton from Core 42. Diffuse lower contact with underlying Dmm diamicton is highlighted (black dashed line). **(d)** Massive, matrix-supported diamicton in Core 44.

Figure 4: Core 42 sedimentary data; **(a)** true-colour photograph; **(b)** X-radiograph structure sketch; red boxes indicate locations of x-radiograph facies examples (Fig. 3b, c); **(c)** sedimentary log including lithofacies codes (Table 2) and calibrated radiocarbon age ranges where applicable (calcareous sample material symbol marks depth below seafloor; refer to Table 5 for specific radiocarbon data). Lithofacies association (LFA) bar correlates with sedimentary data and stratigraphic profile in interpretation section (Fig. 9). Physical and sedimentological properties are plotted against depth. Sand, silt and clay percentages are shown as pie charts, centred at appropriate depth intervals. The smoothed average magnetic susceptibility value is shown as a green line.

Figure 5: Core 43 sedimentary data; **(a)** true-colour photograph; **(b)** X-radiograph structure sketch; **(c)** sedimentary log including lithofacies codes (Table 2). Lithofacies association (LFA) bar correlates with sedimentary data and stratigraphic profile in interpretation section (Fig. 9). Sand, silt and clay percentages are shown as pie charts, centred at appropriate depth intervals. Refer to Figure 4 for legend.

Figure 6: Core 44 sedimentary data; **(a)** true-colour photograph; **(b)** X-radiograph structure sketch; red box indicates location of x-radiograph facies example (Fig. 3d); **(c)** sedimentary log including lithofacies codes (Table 2) and calibrated radiocarbon age ranges where applicable (calcareous sample material symbol marks depth below seafloor; refer to Table 5 for specific radiocarbon data). Lithofacies association (LFA) bar correlates with sedimentary data and stratigraphic profile in discussion section (Fig. 9). Sand, silt and clay percentages are shown as pie charts, centred at appropriate depth intervals. Refer to Figure 4 for legend.

728

729 Figure 7: Core 45 sedimentary data; **(a)** true-colour photograph; **(b)** X-radiograph structure sketch; red box indicates location
 730 of x-radiograph facies example (Fig. 3a); **(c)** sedimentary log including lithofacies codes (Table 2) and calibrated
 731 radiocarbon age ranges where applicable (calcareous sample material symbol marks depth below seafloor; refer to Table 5
 732 for specific radiocarbon data). Lithofacies association (LFA) bar correlates with sedimentary data and stratigraphic profile
 733 in interpretation section (Fig. 9). Physical and sedimentological properties are plotted against depth. Sand, silt and clay
 734 percentages are shown as pie charts, centred at appropriate depth intervals. The smoothed average magnetic susceptibility
 735 value is shown as a green line. Refer to Figure 4 for legend.

736

737 Figure 8: Graphs displaying benthic-foraminifera diversity indices and total-count foraminifera statistics. Calibrated AMS
 738 radiocarbon ages are provided to the left of the diversity plots (Table 4). Stratigraphically-correlated lithofacies and
 739 lithofacies associations are shown on the right. Abbreviations: PTr = percentage of planktonic individuals; SDr = ratio of
 740 severely damaged; LFA = lithofacies association.

741

742 Figure 9: Graphs of relative abundances (shown as a percent along abscissae) for select benthic foraminifera species.
 743 Species are grouped into three palaeoenvironment species groups identified based on modern habitat preferences (see text
 744 for details). Calibrated AMS radiocarbon ages are provided to the left of the abundance plots (Table 4). Note that abscissae
 745 dimensions are only plotted to a relative scale between species to better display changes in species with lower maximum
 746 relative abundances. Abbreviations: LFA = lithofacies association; C. leav. = *C. laevigata*; U. med. = *U. mediterranea*; B.
 747 marg. = *B. marginata*; D. marg. = *D. coronata*; T. angu. = *T. angulosa*; C. reni. = *C. reniforme*; E. clav. = *E. clavatum*.

748

749 Figure 10: Stratigraphic profile showing interpreted facies across transect A-A' (Fig. 2b). Core locations and lithofacies
 750 associations are marked by labelled, vertical bars that correlate with those in Figures 3, 4, 5, 6, 7 and 8. Arrows show
 751 locations of radiocarbon sample acquisition and calibrated results are provided.

752

753 Figure 11: depositional model schematic of glacial history on the Porcupine Bank and Slyne Trough, west of Ireland. **(a)**
 754 Maximum westward extent of BIIS reaches the Porcupine Bank $\leq 24,720 \pm 260$ Cal BP. A terminal moraine/grounding-zone
 755 wedge forms from till. Loose glaciomarine diamicton forms proglacially from sediment plume suspension settling and
 756 sediment rain out (IRD). **(b)** Initial retreat moves ice margin east and uncoupling from the Slyne Trough allows the inflow
 757 of Atlantic water below the BIIS within $24,720 \pm 260$ to $19,182 \pm 155$ Cal BP. Minor readvances create ice shelf push ridges
 758 on the Porcupine Bank. A new grounding-zone wedge forms in the Slyne Trough. Loose glaciomarine diamicton is
 759 deposited proglacially and as sub-ice shelf rain out. Debris flows on the Porcupine Bank ridges are likely. **(c)** Sub-ice shelf
 760 and proglacial diamicton sedimentation continues. Ice shelf thins due to climate amelioration and continued Atlantic water
 761 inflow. Sea level rise and ice thinning causes rapid ice shelf break up $\leq 19,182 \pm 155$ Cal BP, which deposits a clast-rich
 762 glaciomarine diamicton. Increased palaeocurrents winnow the glaciomarine sediment of fines. A new grounding-zone
 763 wedge forms farther to the east in the Slyne Trough. **(d)** Open water conditions emerge following ice shelf break up. A
 764 north-northeastward palaeocurrent concentrates iceberg drift into the Slyne Trough where iceberg keels scour the seafloor
 765 and butt against the southern slopes of grounding-zone wedges, moraines and push ridges. Note that for enhanced clarity,
 766 this schematic simplifies the orientation of Porcupine Bank and Slyne Trough ridges (cf. Fig. 2); also, relative elevations of
 767 ice thickness, sea level and bathymetry are drawn to optimise graphical clarity. Overlying sandy Holocene sediments
 768 deposited postglacially by bottom current reworking are not shown.

769

770 References

771 Alley, R.B., Anandakrishnan, S., Dupont, T.K., Parizek, B.R., Pollard, D. (2007). Effect of
772 sedimentation on ice-sheet grounding-line stability. *Science*, 315(5820), 1838-1841.

773 Amorosi, A., Colalongo, M., Pasini, G., Preti, D. (1999). Sedimentary response to Late Quaternary sea-
774 level changes in the Romagna coastal plain (northern Italy). *Sedimentology*, 46(1), 99-121.

775 Anderson, J.B. (1999). *Antarctic Marine Geology*. Cambridge University Press, Cambridge, 289pp.

776 Anderson, J.B., Brake, C., Domack, E., Myers, N., Wright, R. (1983). Development of a polar glacial-
777 marine sedimentation model from Antarctic Quaternary deposits and glaciological
778 information. In: *Glacial-marine sedimentation*. Springer, US, 233-264.

779 Ballantyne, C.K. (2010). Extent and deglacial chronology of the last British-Irish Ice Sheet:
780 implications of exposure dating using cosmogenic isotopes. *Journal of Quaternary Science*,
781 25(4), 515-534.

782 Barrie, J.V., Conway, K.W. (2002). Rapid sea-level change and coastal evolution on the Pacific
783 margin of Canada. *Sedimentary Geology*, 150(1), 171-183.

784 Bart, P.J., Cone, A.N. (2012). Early stall of West Antarctic Ice Sheet advance on the eastern Ross Sea
785 middle shelf followed by retreat at 27,500 14C BP. *Palaeogeography, Palaeoclimatology*,
786 *Palaeoecology*, 335–336, 52-60.

787 Belderson, R.H., Kenyon, N.H., Wilson, J.B. (1973). Iceberg plough marks in the northeast Atlantic.
788 *Palaeogeography, Palaeoclimatology and Palaeoecology*. 13, 215–224.

789 Benetti, S., Dunlop, P., Ó Cofaigh, C. (2010). Glacial and glacially-related features on the continental
790 margin of northwest Ireland mapped from marine geophysical data. *Journal of Maps*, 6(1),
791 14-29.

792 Berger, W.H., Diester-Haass, L. (1988). Paleoproductivity: the benthic/planktonic ratio in foraminifera
793 as a productivity index. *Marine Geology*. 81, 15-25.

794 Bishop, P., Jones, E.J.W. (1979). Patterns of glacial and post-glacial sedimentation in the Minches,
795 North-West Scotland. *Elsevier Oceanography Series*, 24, 89-194.

796 Bouchet, V.M., Alve, E., Rygg, B., Telford, R.J. (2012). Benthic foraminifera provide a promising
797 tool for ecological quality assessment of marine waters. *Ecological indicators*, 23, 66-75.

798 Boulton, G.S. (1986). Push-moraines and glacier-contact fans in marine and terrestrial
799 environments. *Sedimentology*, 33, 677-698.

800 Bradwell, T., Stoker, M.S., Golledge, N.R., Wilson, C.K., Merritt, J.W., Long, D., Everest, J.D.,
801 Hestvik, O.B., Stevenson, A.G., Hubbard, A.I., Finlayson, A.G., Mathers, H.E. (2008). The
802 northern sector of the last British Ice Sheet: maximum extent and demise. *Earth-Science*
803 *Reviews*, 88(3), 207-226.

804 Buzas, M. A., Gibson, T. G. (1969). Species diversity: benthonic foraminifera in western North
805 Atlantic. *Science*, 163(3862), 72-75.

806 Carmack, E., Wassmann, P. (2006). Food webs and physical-biological coupling on pan-Arctic
807 shelves: unifying concepts and comprehensive perspectives. *Progress in Oceanography*,
808 71(2-4), 446-477.

809 Clark, J., McCabe, A., Schnabel, C., Clark, P.U., Freeman, S., Maden, C., Xu, S. (2009). ¹⁰Be
810 chronology of the last deglaciation of County Donegal, northwestern Ireland. *Boreas*, 38(1),
811 111-118.

812 Clark, C.D., Hughes, A.L.C., Greenwood, S.L., Jordan, C., Sejrup, H.P. (2012a). Pattern and timing
813 of retreat of the last British-Irish Ice Sheet. *Quaternary Science Reviews*, 44, 112-146.

814 Clark, J., McCabe, A.M., Bowen, D.Q., Clark, P.U. (2012b). Response of the Irish Ice Sheet to abrupt
815 climate change during the last deglaciation. *Quaternary Science Reviews*, 35, 100-115.

816 Conway, H., Hall, B., Denton, G., Gades, A., Waddington, E. (1999). Past and future grounding-line
817 retreat of the West Antarctic ice sheet. *Science*, 286(5438), 280-283.

818 d'Orbigny, A. (1847). Voyage dans l'Amérique Méridionale... exécuté pendant les années 1826-1833
819 (Vol. 1).

820 De Haas, H., Mienis, F., Frank, N., Richter, T., Steinacher, R., De Stigter, H., Vander Land, C., Van Weering, T.
821 (2009). Morphology and sedimentology of (clustered) cold-
822 water coral mounds at the south Rockall Trough margins, NE Atlantic Ocean. *Facies*, 55, 1–26.

823 Diester-Haass, L. (1978). Sediments as indicators of upwelling. In: *Upwelling ecosystems*. Boje,
824 R., Tomczak, M. (Eds). Springer, Heidelberg, 261-281.

825 Domack, E., Duran, D., Leventer, A., Ishman, S., Doanne, S., McCallum, S., Amblas, D., Ring, J.,
826 Gilbert, R., Prentice, M. (2005). Stability of the Larsen B ice shelf on the Antarctic Peninsula
827 during the Holocene epoch. *Nature*, 436, 681–685.

828 Dorst, S., Schönfeld, J. (2013). Diversity of benthic foraminifera on the shelf and slope of the NE
829 Atlantic: analysis of datasets. *The Journal of Foraminiferal Research*, 43(3), 238-254.

830 Dowdeswell, J. A., Fugelli, E. M. G. (2012). The seismic architecture and geometry of grounding-zone
831 wedges formed at the marine margins of past ice sheets. *Geological Society of America*
832 *Bulletin*, 124(11-12), 1750-1761.

833 Dowdeswell, J.A., Villinger, H., Whittington, R.J., Marienfeld, P. (1993). Iceberg scouring in
834 Scoresby Sund and on the East Greenland continental shelf. *Marine Geology*. 111, 37–53.

835 Dowdeswell, J., Ottesen, D., Evans, J., Ó Cofaigh, C., Anderson, J. (2008). Submarine glacial
836 landforms and rates of ice-stream collapse. *Geology*, 36(10), 819-822.

837 Dunlop, P., Shannon, R., McCabe, M., Quinn, R., Doyle, E. (2010). Marine geophysical evidence for
838 ice sheet extension and recession on the Malin Shelf: New evidence for the western limits of
839 the British Irish Ice Sheet. *Marine Geology*, 276(1), 86-99.

840 Evans, J., Pudsey, C.J. (2002). Sedimentation associated with Antarctic Peninsula ice shelves:
841 implications for palaeoenvironmental reconstructions of glacialmarine sediments. *Journal of*
842 *the Geological Society*, 159(3), 233-237.

843 Evans, D.J.A., O'Cofaigh, C. (2003). Depositional evidence for marginal oscillations of the Irish Sea
844 ice stream in southeast Ireland during the last glaciation. *Boreas*, 32(1), 76-101.

845 Evans, J., Pudsey, C.J., Ó Cofaigh, C., Morris, P., Domack, E. (2005). Late Quaternary glacial
846 history, flow dynamics and sedimentation along the eastern margin of the Antarctic Peninsula
847 ice sheet. *Quaternary science reviews*, 24, 741– 774.

848 Eyles, C.H. (1988). A model for striated boulder pavement formation on glaciated, shallow-marine
849 shelves: an example from the Yakataga Formation, Alaska. *Journal of Sedimentary Research*,
850 58(1), 62-71.

851 Eyles, N., Eyles, C.H., Miall, A.D. (1983). Lithofacies types and vertical profile models; an
852 alternative approach to the description and environmental interpretation of glacial diamict and
853 diamictite sequences. *Sedimentology*, 30(3), 393-410.

854 Feyling-Hanssen, R.W. (1972). The foraminifer *Elphidium excavatum* (Terquem) and its variant
855 forms. *Micropaleontology*, 18(3), 337-354.

856 Fisher, R.A., Corbet, A.S., Williams, C.B. (1943). The relationship between the number of species and
857 the number of individuals in a random sample of animal population. *Journal of Animal*
858 *Ecology*, 12, 42–58.

859 Fyfe, J.A., Long, D. Evans, D. (1993) The geology of the Malin-Hebrides Sea area. *British Geological*
860 *Survey, United Kingdom, Offshore Regional Report*. HMSO, London.

861 García, M., Ercilla, G., Alonso, B., Casas, D., Dowdeswell, J.A. (2011). Sediment lithofacies,
862 processes and sedimentary models in the Central Bransfield Basin, Antarctic Peninsula, since
863 the Last Glacial Maximum. *Marine Geology*, 290(1), 1-16.

864 Gladstone, R.M., Lee, V., Rougier, J., Payne, A.J., Hellmer, H., Le Brocq, A., Cornford, S. L.
865 (2012). Calibrated prediction of Pine Island Glacier retreat during the 21st and 22nd centuries
866 with a coupled flowline model. *Earth and Planetary Science Letters*, 333, 191-199.

867 Glasser, N. F., Scambos, T. A., Bohlander, J., Truffer, M., Pettit, E., Davies, B. J. (2011). From ice-
868 shelf tributary to tidewater glacier: continued rapid recession, acceleration and thinning of
869 Röhss Glacier following the 1995 collapse of the Prince Gustav Ice Shelf, Antarctic
870 Peninsula. *Journal of Glaciology*, 57(203), 397-406.

871 Gooday, A.J., Hughes, J.A. (2002). Foraminifera associated with phytodetritus deposits
872 at a bathyal site in the northern Rockall Trough (NE Atlantic): seasonal contrasts
873 and a comparison of stained and dead assemblages. *Marine Micropaleontology*, 46, 83–110.

874 Greenwood, S.L., Clark, C.D. (2009). Reconstructing the last Irish Ice Sheet 2: a geomorphologically-
875 driven model of ice sheet growth, retreat and dynamics. *Quaternary Science Reviews*, 28(27-
876 28), 3101-3123.

877 Grobe, H. (1987). A simple method for the determination of ice-rafted debris in sediment
878 cores. *Polarforschung*, 57(3), 123-126.

879 Hald, M., Korsun, S. (1997). Distribution of modern benthic foraminifera from fjords of
880 Svalbard, European Arctic. *Journal of Foraminiferal Research*. 27(2), 101–122.

881 Hald, M., Vorren, T.O. (1987). Foraminiferal stratigraphy and environment of Late
882 Weichselian deposits on the continental shelf off Troms, Northern Norway. *Marine*
883 *Micropaleontology*, 12, 129–160.

884 Hald, M., Sættem, J., Nesse, E. (1990). Middle and Late Weichselian stratigraphy in shallow drillings
885 from the southwestern Barents Sea: foraminiferal, amino acid and radiocarbon evidence.
886 *Norsk Geologisk Tidsskrift*, 70(4), 241-257.

- 887 Hald, M., Steinsund, P.I., Dokken, T., Korsun, S., Polyak, L., Aspeli, R. (1993). Recent and Late
888 Quaternary distribution of *Elphidium excavatum* f. *clavata* in Arctic seas. *Cushman*
889 *Foundation Sp. Publication*, 32, 141-153.
- 890 Hald, M., Steinsund, P.I., Dokken, T., Korsun, S., Polyak, L., Aspeli, R., (1994). Recent and late
891 Quaternary distribution of *Elphidium excavatum* f. *clavata* in Arctic seas. *Cushman*
892 *Foundation Special Publication*, 32, 141-153.
- 893 Hammer, Ø., Harper, D.A.T., Ryan, P.D. (2001). PAST: Paleontological Statistics Software
894 Package for Education and Data Analysis. *Palaeontologia Electronica*, 4(1): 9pp.
- 895 Hebbeln, D., Wefer, G. (1991). Effects of ice coverage and ice-rafted material on sedimentation in the
896 Fram Strait. *Nature*, 350, 409-411.
- 897 Hein, F.J., Syvitski, J.P.M. (1992). Sedimentary environments and facies in an Arctic basin, Itirbilung
898 Fiord, Baffin Island, Canada. *Sedimentary Geology*, 81, 17-45.
- 899 Heindel, K., Titschack, J., Dorschel, B., Huvenne, V.A., Freiwald, A. (2010). The sediment
900 composition and predictive mapping of facies on the Propeller Mound—A cold-water coral
901 mound (Porcupine Seabight, NE Atlantic). *Continental Shelf Research*, 30(17), 1814-1829.
- 902 Heinrich, H. (1988). Origin and consequences of cyclic ice rafting in the northeast Atlantic Ocean
903 during the past 130,000 years. *Quaternary research*, 29(2), 142-152.
- 904 Hillenbrand, C.D., Baesler, A., Grobe, H. (2005). The sedimentary record of the last glaciation in the
905 western Bellingshausen Sea (West Antarctica): implications for the interpretation of
906 diamictos in a polar-marine setting. *Marine geology*, 216(4), 191-204.
- 907 Hillenbrand, C.D., Larter, R.D., Dowdeswell, J.A., Ehrmann, W., Ó Cofaigh, C., Benetti, S., Grobe,
908 H. (2010). The sedimentary legacy of a palaeo-ice stream on the shelf of the southern
909 Bellingshausen Sea: Clues to West Antarctic glacial history during the Late Quaternary.
910 *Quaternary Science Reviews*, 29(19), 2741-2763.

911 Hillenbrand, C.-D., Kuhn, G., Smith, J.A., Gohl, K., Graham, A.G., Larter, R.D., Klages, J.P.,
912 Downey, R., Moreton, S.G., Forwick, M., Vaughan, D.G. (2013). Grounding-line retreat of
913 the west Antarctic ice sheet from inner Pine island Bay. *Geology*, 41(1), 35-38.

914 Hofker, J., 1930. Notizenüber die Foraminiferen des Golfes von Neapel.
915 *PubblicazionidellaStazioneZoologica di Napoli*, 10(3), 366-406.

916 Hubbard, A., Bradwell, T., Golledge, N., Hall, A., Patton, H., Sugden, D., Cooper, R., Stoker, M.
917 (2009).Dynamic cycles, ice streams and their impact on the extent, chronology and
918 deglaciation of the British–Irish ice sheet.*Quaternary Science Reviews*, 28(7), 758-776.

919 Jakobsson, M., Anderson, J.B., Nitsche, F.O.,Gyllencreutz, R., Kirshner, A.E., Kirchner, N.,
920 O'Regan, M., Mohammad, R., Eriksson, B. (2012). Ice sheet retreat dynamics inferred from
921 glacial morphology of the central Pine Island Bay Trough, West Antarctica. *Quaternary*
922 *Science Reviews*, 38, 1-10.

923 Jennings, A.E., Walton, M.E., Ó Cofaigh, C., Kilfeather, A., Andrews, J.T., Ortiz, J.D., De Vernal,
924 A., Dowdeswell, J.A. (2014). Paleoenvironments during Younger Dryas-Early Holocene
925 retreat of the Greenland Ice Sheet from outer Disko Trough, central west Greenland. *Journal*
926 *of Quaternary Science*, 29(1), 27-40.

927 Joughin, I., Abdalati, W.,Fahnestock, M. (2004).Large fluctuations in speed on Greenland's
928 JakobshavnIsbrae glacier.*Nature*, 432(7017), 608-610.

929 Kilfeather, A.A., Ó Cofaigh, C., Lloyd, J.M., Dowdeswell, J.A., Xu, S., Moreton, S.G. (2011). Ice-
930 stream retreat and ice-shelf history in Marguerite Trough, Antarctic Peninsula:
931 Sedimentological and foraminiferal signatures. *Geological Society of America Bulletin*,
932 123(5-6), 997-1015.

933 King, E.L., Haflidason, H., Sejrup, H.P., Austin, W.E.N., Duffey, M., Helland, H., Klitgaard-
934 Kristensen, D., Scourse, J. (1998). End Moraines on the Northwest Irish Continental Shelf.
935 *Third ENAM IIWorkshop*, Edinburgh, (abstract volume).

- 936 Klitgaard Kristensen, D., Serjup, H.P. (1996). Modern benthic foraminiferal biofacies across
937 the northern North Sea. *Sarsia*, 81, 97–106.
- 938 Kuchar, J., Milne, G., Hubbard, A., Patton, H., Bradley, S., Shennan, I., Edwards, R. (2012).
939 Evaluation of a numerical model of the British–Irish ice sheet using relative sea-level data:
940 implications for the interpretation of trimline observations. *Journal of Quaternary Science*,
941 27(6), 597–605.
- 942 Linke, P., Lutze, G.F. (1993). Microhabitat preferences of benthic foraminifera—a static concept or a
943 dynamic adaptation to optimize food acquisition? *Marine Micropaleontology*, 20(3), 215–234.
- 944 Lowe, A. L., Anderson, J. B. (2003). Evidence for abundant subglacial meltwater beneath the paleo-
945 ice sheet in Pine Island Bay, Antarctica. *Journal of Glaciology*, 49(164), 125–138.
- 946 Mackensen, A., Fütterer, D.K., Grobe, H., Schmiedl, G. (1993). Benthic foraminiferal assemblages
947 from the eastern South Atlantic Polar Front region between 351 and 571 S:
948 distribution, ecology and fossilization potential. *Marine Micropaleontology*, 22, 33–69.
- 949 Mazzini, A., Akhmetzhanov, A., Monteys, X., Ivanov, M. (2012). The Porcupine Bank Canyon coral
950 mounds: oceanographic and topographic steering of deep-water carbonate mound
951 development and associated phosphatic deposition. *Geo-Marine Letters*, 32(3), 205–225.
- 952 Melis, R., Salvi, G. (2009). Late Quaternary foraminiferal assemblages from western Ross Sea
953 (Antarctica) in relation to the main glacial and marine lithofacies. *Marine Micropaleontology*,
954 70(1–2), 39–53.
- 955 Miall, A.D. (1978). Lithofacies types and vertical profile models in braided rivers: a summary. In:
956 *Fluvial Sedimentology* (Ed. by A.D. Miall). Memoirs of the Canadian Society of Petroleum
957 Geologists, 5, 597–604.

958 Mojtabid, M., Jorissen, F., Lansard, B., Fontanier, C., Bombled, B., Rabouille, C. (2009). Spatial
959 distribution of live benthic foraminifera in the Rhône prodelta: Faunal response to a
960 continental–marine organic matter gradient. *Marine Micropaleontology*, 70(3), 177-200.

961 Morigi, C., Sabbatini, A., Vitale, G., Pancotti, I., Gooday, A. J., Duineveld, G. C. A., De
962 Stigter, H. C., Danavaro, R., Negri, A. (2012). Foraminiferal biodiversity associated with cold-
963 water coral carbonate mounds and open slope of SE Rockall Bank (Irish continental margin—NE
964 Atlantic). *Deep-Sea Research*, 59, 54–71.

965 Mudie, P. J., Keen, C. E., Hardy, I. A., Vis, G. (1984). Multivariate analysis and quantitative
966 paleoecology of benthic foraminifera in surface and Late Quaternary shelf sediments, northern
967 Canada. *Micropaleontology*, 8, 283-313.

968 Murphy, N. J., Croker, P. F. (1992). Many play concepts seen over wide area in Erris, Slyne troughs off
969 Ireland. *Oil and Gas*, 90(37), 92-97.

970 Murray, J. W. (1991). *Ecology and palaeoecology of benthic foraminifera*. Longman Scientific &
971 Technical, New York, 397pp.

972 Murray, J. W. (2003). An illustrated guide to the benthic foraminifera of the Hebridean shelf, west of
973 Scotland, with notes on their mode of life. *Palaeontologia Electronica*, 5(1), 31.

974 Murray, J. W. (2006). *Ecology and application of benthic foraminifera*. Cambridge University Press,
975 Cambridge, 422pp.

976 Nørvang, A. (1945). *Foraminifera*: Ejnar Munksgaard.

977 Ó Cofaigh, C., Dowdeswell, J. A. (2001). Laminated sediments in glacial marine environments:
978 diagnostic criteria for their interpretation. *Quaternary Science Reviews*, 20(13), 1411-1436.

979 Ó Cofaigh, C., Evans, D. J. (2007). Radiocarbon constraints on the age of the maximum advance of
980 the British–Irish Ice Sheet in the Celtic Sea. *Quaternary Science Reviews*, 26(9), 1197-1203.

981 Ó Cofaigh, C., Taylor, J., Dowdeswell, J.A., Rosell-Mele, A., Kenyon, N.H., Evans, J., Mienert, J.
 982 (2002). Geological evidence for sediment reworking on high-latitude continental margins and
 983 its implications for palaeoceanography: insights from the Norwegian-Greenland Sea. In:
 984 Dowdeswell, J.A., Ó Cofaigh, C. (Eds.), *Glacier-influenced Sedimentation on High-latitude*
 985 *Continental Margins. Geological Society of London, Special Publication*, 203, 325–348.

986 Ó Cofaigh, C., Dowdeswell, J.A., Allen, C.S., Hiemstra, J.F., Pudsey, C.J., Evans, J., Evans, D.J.A.
 987 (2005). Flow dynamics and till genesis associated with a marine-based Antarctic palaeo-
 988 ice stream. *Quaternary Science Reviews*, 24, 709–740.

989 Ó Cofaigh, C., Dunlop, P., Benetti, S. (2010). Marine geophysical evidence for Late Pleistocene ice
 990 sheet extent and recession off northwest Ireland. *Quaternary Science Reviews*, 44, 147–159.

991 Ó Cofaigh, C., Evans, D.J.A., Hiemstra, J.F. (2011). Formation of a stratified subglacial ‘till’
 992 assemblage by ice-marginal thrusting and glacier overriding. *Boreas*, 40(1), 1–14.

993 Ovenshine, A.T. (1970). Observations of iceberg rafting in Glacier Bay, Alaska, and the identification
 994 of ancient ice-rafted deposits. *Geological Society of America Bulletin*, 81(3), 891–894.

995 Ovsepyan, E.A., Ivanova, E.V., Max, L., Riethdorf, J.R., Nürnberg, D., Tiedemann, R. (2013). Late
 996 quaternary oceanographic conditions in the Western Bering Sea. *Oceanology*, 53(2), 211–222.

997 Park, J.W., Gourmelen, N., Shepherd, A., Kim, S.W., Vaughan, D.G., Wingham, D.J.
 998 (2013). Sustained retreat of the Pine Island Glacier. *Geophysical Research Letters*, 40(10)
 999 2137–2142.

1000 Parker, W.K., Jones, T.R., Bailey, J., Pourtales, F. (1865). On some foraminifera from the north
 1001 Atlantic and Arctic Oceans, including Davis Straits and Baffin's Bay. *Philosophical*
 1002 *Transactions of the Royal Society of London*, 325–441.

- 1003 Peck, V., Hall, I., Zahn, R., Elderfield, H., Grousset, F., Hemming, S., Scourse, J. (2006). High
1004 resolution evidence for linkages between NW European ice sheet instability and Atlantic
1005 Meridional Overturning Circulation. *Earth and Planetary Science Letters*, 243(3), 476-488.
- 1006 Pfeffer, W.T. (2007). A simple mechanism for irreversible tidewater glacier retreat. *Journal of*
1007 *Geophysical Research: Earth Surface*, 112, F03S25.
- 1008 Polyak, L., Gataullin, V., Gainanov, V., Gladyshev, V., Goremykin, Yu. (2002). Kara Sea
1009 expedition yields insight into LGM ice sheet extent. *Eos* 83, 46, 525-529.
- 1010 Powell, R.D. (1983). Glacial-marine sedimentation processes and lithofacies of temperate tidewater
1011 glaciers, Glacier Bay, Alaska. In: Molnia, B.F. (Ed.), *Glacial-Marine Sedimentation*. Plenum
1012 Press, New York, 195-232.
- 1013 Pritchard, H.D., Arthern, R.J., Vaughan, D.G., Edwards, L.A. (2009). Extensive dynamic thinning on
1014 the margins of the Greenland and Antarctic ice sheets. *Nature*, 461(7266), 971-975.
- 1015 Pudsey, C.J., Evans, J. (2001). First survey of Antarctic sub-ice shelf sediments reveals mid-Holocene
1016 ice shelf retreat. *Geology*, 29, 787-790.
- 1017 Ren, D., Leslie, L.M., Lynch, M.J. (2013). Verification of model simulated mass balance, flow fields
1018 and tabular calving events of the Antarctic ice sheet against remotely sensed observations.
1019 *Climate Dynamics*, (40), 2617-2636.
- 1020 Rignot, E., Casassa, G., Gogineni, P., Krabill, W., Rivera, A.U., Thomas, R. (2004). Accelerated ice
1021 discharge from the Antarctic Peninsula following the collapse of Larsen B ice
1022 shelf. *Geophysical Research Letters*, 31(18), 1-4.
- 1023 Robinson, S.G., Maslin, M.A., McCave, I.N. (1995). Magnetic susceptibility variations in late
1024 Pleistocene deep-sea sediments of the N.E. Atlantic: implications for ice-rafting and
1025 paleocirculation at the last Glacial Maximum. *Paleoceanography*, 10, 221-250.

- 1026 Rott, H., Rack, W., Skvarca, P., De Angelis, H. (2002). Northern Larsen Ice Shelf, Antarctica: further
1027 retreat after collapse. *Annals of Glaciology*, 34, 277–282.
- 1028 Sacchetti, F., Benetti, S., Georgiopoulou, A., Shannon, P.M., O'Reilly, B.M., Dunlop, P., O'Cofaigh,
1029 C. (2012). Deep-water geomorphology of the glaciated Irish margin from high-resolution
1030 marine geophysical data. *Marine Geology*, 291, 113–131.
- 1031 Saito, Y., Katayama, H., Ikehara, K., Kato, Y., Matsumoto, E., Oguri, K., Oda, M., Yumoto, M.
1032 (1998). Transgressive and highstand systems tracts and post-glacial transgression, the East
1033 China Sea. *Sedimentary Geology*, 122(1), 217–232.
- 1034 Samir, A.M., Abdou, H.F., Zazou, S.M., El-Menhawey, W.H. (2003). Cluster analysis of recent
1035 benthic foraminifera from the northwestern Mediterranean coast of Egypt. *Revue de*
1036 *Micropaléontologie*, 46(2), 111–130.
- 1037 Scambos, T.A., Bohlander, J.A., Shuman, C.U., Skvarca, P. (2004). Glacier acceleration and thinning
1038 after ice shelf collapse in the Larsen B embayment, Antarctica. *Geophysical Research Letters*,
1039 31(18), 1–4.
- 1040 Schönfeld, J. (1997). The impact of the Mediterranean Outflow Water (MOW) on benthic
1041 foraminiferal assemblages and surface sediments at the southern Portuguese margin. *Marine*
1042 *Micropaleontology*, 29, 211–236.
- 1043 Schönfeld, J. (2002). A new benthic foraminiferal proxy for near-bottom current velocities in the Gulf
1044 of Cadiz, northeastern Atlantic Ocean. *Deep Sea Research Part I: Oceanographic Research*
1045 *Papers*, 49(10), 1853–1875.
- 1046 Schönfeld, J., Alve, E., Geslin, E., Jorissen, F., Korsun, S., Spezzaferri, S. (2012). The FOBIMO
1047 (FORaminiferal BIO-MONitoring) initiative—Towards a standardised protocol for soft-bottom
1048 benthic foraminiferal monitoring studies. *Marine Micropaleontology*, 94, 1–13.

- 1049 Schwab, W.C., Lee, H.J., Twichell, D.C., Locat, J., Nelson, C.H., McArthur, W.G., Kenyon, N.H.
 1050 (1996). Sediment mass-flow processes on a depositional lobe, outer Mississippi Fan. *Journal*
 1051 *of Sedimentary Research*, 66(5), 916-926.
- 1052 Scoffin, T.P., Bowes, G.E. (1988). The facies distribution of carbonate sediments on Porcupine Bank,
 1053 northeast Atlantic. *Sedimentary geology*, 60(1), 125-134.
- 1054 Scourse, J.D., Haapaniemi, A.I., Colmenero-Hidalgo, E., Peck, V.L., Hall, I.R., Austin, W.E., Knutz,
 1055 P.C., Zahn, R. (2009). Growth, dynamics and deglaciation of the last British–Irish ice sheet:
 1056 the deep-sea ice-rafted detritus record. *Quaternary Science Reviews*, 28(27), 3066-3084.
- 1057 Sejrup, H.P., Guilbault, J.P. (1980). *Cassidulina reniforme* and *C. obtusa* (Foraminifera), taxonomy,
 1058 distribution, and ecology: *Sarsia*, 65, 79-85.
- 1059 Sejrup, H.P., Birks, H.J.B., Klitgaard Kristensen, D., Madsen, H. (2004). Benthonic foraminiferal
 1060 distributions and quantitative transfer functions for the northwest European continental
 1061 margin. *Marine Micropaleontology*, 53, 197-226.
- 1062 Sejrup, H.P., Hjelstuen, B.O., Dahlgren, K.I.T., Haflidason, H., Kuijpers, A., Nygård, A., Praeg, D.,
 1063 Stoker, M.S., Vorren, T.O. (2005). Pleistocene glacial history of the NW European
 1064 continental margin. *Marine and Petroleum Geology*, 22, 1111–1129.
- 1065 Sharp, M. (1982). Modification of clasts in lodgement tills by glacial erosion. *Journal of Glaciology*,
 1066 28(100), 475-481.
- 1067 Shevenell, A.E., Domack, E.W., Kernan, G.M. (1996). Record of Holocene palaeoclimate change
 1068 along the Antarctic Peninsula: evidence from glacial marine sediments, Lallemand Fjord.
 1069 *Papers and Proceedings of the Royal Society of Tasmania*, 130(2), 55-64.
- 1070 Smeulders, G.G.B., Koho, K.A., de Stigter, H.C., Mienis, F., de Haas, H., van Weering, T.C.E.
 1071 (2014). Cold-water coral habitats of Rockall and Porcupine Bank, NE Atlantic Ocean:

1072 Sedimentary facies and benthic foraminiferal assemblages.*Deep Sea Research Part II:*
1073 *Topical Studies in Oceanography*, 99, 270-285.

1074 Smith, J.A., Hillenbrand, C.D., Kuhn, G., Larter, R.D., Graham, A.G., Ehrmann, W., Moreton, S.G.,
1075 Forwick, M. (2011). Deglacial history of the West Antarctic Ice Sheet in the western
1076 Amundsen Sea embayment. *Quaternary Science Reviews*, 30(5), 488-505.

1077 Stalder, C., Spezzaferri, S., Rüggeberg, A., Pirkenseer, C., Gennari, G. (2014). Late Weichselian
1078 deglaciation and early Holocene development of a cold-water coral reef along the Lopphavet
1079 shelf (Northern Norway) recorded by benthic foraminifera and ostracoda. *Deep Sea Research*
1080 *Part II: Topical Studies in Oceanography*, 99, 249-269.

1081 Stuiver, M., Reimer, P. J. (1993). Extended 14C database and revised CALIB radiocarbon calibration
1082 program. *Radiocarbon*, 35, 215-230.

1083 Thomas, E., Booth, L., Maslin, M., Shackleton, N. J. (1995). Northeastern Atlantic benthic
1084 foraminifera during the last 45,000 years: changes in productivity seen from the bottom up.
1085 *Paleoceanography*, 10(3), 545-562.

1086 Viana, A., Faugères, J.-C., Stow, D. (1998). Bottom-current-controlled sand deposits—a review of
1087 modern shallow-to deep-water environments. *Sedimentary Geology*, 115(1), 53-80.

1088 Vorren, T.O., Hald, M., Edvardsson, Lind-Hansen, O.W. (1983). Glacigenic sediments and
1089 sedimentary environments on continental shelves: general principles with a case study from the
1090 Norwegian shelf. In: *Glacial Deposits in North- West Europe*. Ehlers, J. (Ed.), pp. 61-73.
1091 Balkema, Rotterdam.

1092 Weston, J.F. (1985). Comparison between recent benthic foraminiferal faunas of the Porcupine
1093 Seabight and western approaches continental slope. *Journal of Micropalaeontology*, 4(2), 165-
1094 183.

1095 Wilson, L. J., Austin, W. E., Jansen, E. (2002). The last British Ice Sheet: growth, maximum extent
1096 and deglaciation. *Polar Research*, 21(2), 243-250.

1097

1098

1099 **Appendix 1**

1100 Table A1: foraminiferal diversity index data.

Core	Interval (cm bsf)	SDr (%)	PTr (%)	Fisher's α	Dominance
42	36	18.04878	63.41463	5.304	0.1363
	58	9.973046	68.46361	5.232	0.1668
	66	12.97539	65.43624	4.785	0.379
	78	35.76159	21.52318	3.879	0.2627
	88	36.02484	65.99379	2.729	0.2584
	108	27.0979	56.46853	3.508	0.2968
	139	17.29323	59.54887	3.134	0.3251
	157	22.51256	50.25126	2.677	0.2335
43	28	13.66806	70.99024	4.04	0.1893
	44	17.24138	74.03017	5.53	0.2773
	65	11.78248	66.76737	4.639	0.2629
	85	16.66667	63.4058	2.794	0.3835
44	5	8.726415	56.25	3.948	0.1325
	27	10.36107	60.75353	4.772	0.1207
	46	16.15799	56.55296	5.872	0.1156
	80	12.66376	56.55022	5.533	0.1685
	120	8.439898	47.82609	5.872	0.1908
	139	16.08775	52.10238	5.382	0.1622
	180	25.15723	53.45912	5.702	0.1892
	223	19.7561	50.4878	5.916	0.1626
45	31	10.25358	53.47299	4.365	0.1465
	57	16.61491	48.91304	4.993	0.1229
	94	13.53383	48.87218	6.272	0.1076
	142	8.523909	54.67775	5.759	0.1265
	254	12.36559	51.43369	5.328	0.1129

1101

1102

1103 Table A2: Benthic foraminifera absolute abundances (number of individuals) and general micropaleontological data for
 1104 cores 42 and 43. Species with >2% relative abundance in in at least one core (42, 43, 44, 45) in bold, >5% in bold and
 1105 underlined. (Refer to Table A3 for core 44 and 45 data.)

Cm (bsf)	Core 42								Core 43			
	36	58	66	78	88	108	139	157	28	44	65	85
Species	Individuals								Individuals			
<i>Amphicoryna scalaris</i>	0	0	0	0	0	0	0	0	0	0	0	0
<i>Bigenerinanosaria</i>	2	0	0	0	0	0	0	0	0	1	1	0
<i>Buccella frigida</i>	1	0	0	3	0	0	0	0	0	0	0	0
<i>Bulimina elongata</i>	0	0	0	0	0	0	0	0	0	0	1	0
<u>Bulimina gibba</u>	<u>2</u>	<u>1</u>	<u>2</u>	<u>1</u>	<u>0</u>	<u>1</u>	<u>1</u>	<u>0</u>	<u>2</u>	<u>2</u>	<u>5</u>	<u>1</u>
<u>Bulimina marginata</u>	<u>6</u>	<u>8</u>	<u>1</u>	<u>2</u>	<u>1</u>	<u>2</u>	<u>3</u>	<u>2</u>	<u>10</u>	<u>7</u>	<u>6</u>	<u>4</u>
<i>Bulivina sp.</i>	1	2	2	0	0	0	0	0	0	3	0	0
<u>Cassidulina laevigata</u>	<u>27</u>	<u>19</u>	<u>10</u>	<u>2</u>	<u>3</u>	<u>15</u>	<u>24</u>	<u>70</u>	<u>27</u>	<u>14</u>	<u>2</u>	<u>3</u>
<u>Cassidulina obtuse</u>	<u>9</u>	<u>12</u>	<u>17</u>	<u>0</u>	<u>0</u>	<u>1</u>	<u>2</u>	<u>1</u>	<u>15</u>	<u>1</u>	<u>0</u>	<u>0</u>
<u>Cassidulina reniforme</u>	<u>8</u>	<u>3</u>	<u>1</u>	<u>4</u>	<u>2</u>	<u>3</u>	<u>6</u>	<u>7</u>	<u>2</u>	<u>5</u>	<u>6</u>	<u>3</u>
<u>Cibicides lobatula</u>	<u>46</u>	<u>59</u>	<u>183</u>	<u>101</u>	<u>67</u>	<u>65</u>	<u>61</u>	<u>46</u>	<u>66</u>	<u>63</u>	<u>106</u>	<u>113</u>
<u>Cibicides refulgens</u>	<u>38</u>	<u>45</u>	<u>15</u>	<u>40</u>	<u>35</u>	<u>15</u>	<u>3</u>	<u>104</u>	<u>2</u>	<u>5</u>	<u>12</u>	<u>13</u>
<i>Cibicoides pachyderma</i>	0	0	0	0	0	1	2	0	1	0	0	3
<i>Dentalina subsoluta</i>	0	0	0	1	0	0	0	0	0	0		0
<u>Discanomalina coronata</u>	<u>4</u>	<u>6</u>	<u>6</u>	<u>50</u>	<u>12</u>	<u>13</u>	<u>10</u>	<u>31</u>	<u>3</u>	<u>4</u>	<u>17</u>	<u>8</u>
<i>Eggerella bradyi</i>	0	0	1	0	0	0	0	0	0	0	0	0
<u>Elphidium excavatum clavatum</u>	<u>0</u>	<u>1</u>	<u>2</u>	<u>0</u>	<u>0</u>	<u>0</u>	<u>0</u>	<u>0</u>	<u>1</u>	<u>0</u>	<u>0</u>	<u>0</u>
<u>Elphidium excavatum selseyensis</u>	<u>0</u>	<u>1</u>	<u>3</u>	<u>2</u>	<u>0</u>	<u>0</u>	<u>0</u>	<u>0</u>	<u>1</u>	<u>0</u>	<u>0</u>	<u>0</u>
<i>Fissurina sp.</i>	3	3	0	0	0	0	0	0	2	1	1	0
<i>Gavelinopsis translucens</i>	0	0	0	0	1	0	0	0	0	0	0	0
<u>Globocassidulina subglobosa</u>	<u>2</u>	<u>0</u>	<u>1</u>	<u>1</u>	<u>5</u>	<u>2</u>	<u>2</u>	<u>4</u>	<u>1</u>	<u>2</u>	<u>1</u>	<u>0</u>
<i>Guttulina sp.</i>	0	0	0	0	0	0	0	0	0	0	0	1
<u>Gyroidinoides soldanii</u>	<u>0</u>	<u>1</u>	<u>0</u>	<u>0</u>	<u>1</u>	<u>0</u>	<u>1</u>	<u>16</u>	<u>0</u>	<u>0</u>	<u>0</u>	<u>0</u>
<i>Hyalinea balthica</i>	0	0	0	0	0	0	0	0	0	0	0	0
<i>Lagena sp.</i>	0	1	0	0	0	0	0	2	0	1	0	0
<i>Lagena striata</i>	0	0	0	1	0	1	1	0	0	1	1	0
<u>Lenticulina sp.</u>	<u>1</u>	<u>0</u>	<u>0</u>	<u>1</u>	<u>0</u>	<u>0</u>	<u>0</u>	<u>0</u>	<u>0</u>	<u>1</u>	<u>7</u>	<u>0</u>
<u>Melonis barleeanus</u>	<u>0</u>	<u>3</u>	<u>3</u>	<u>0</u>	<u>0</u>	<u>2</u>	<u>0</u>	<u>5</u>	<u>3</u>	<u>3</u>	<u>0</u>	<u>0</u>
<i>Millammina fusca</i>	0	0	0	0	0	0	0	0	0	0	1	0
<i>Millolinella chukchiensis</i>	0	0	0	0	0	0	0	0	0	0	0	0
<i>Nonionella turgida</i>	1	1	2	0	0	0	0	0	0	0	0	0
<i>Oolina caudigera</i>	0	0	0	0	0	0	0	0	0	1	0	0
<u>Planulina ariminensis</u>	<u>3</u>	<u>1</u>	<u>2</u>	<u>0</u>	<u>0</u>	<u>2</u>	<u>0</u>	<u>2</u>	<u>4</u>	<u>3</u>	<u>0</u>	<u>0</u>
<i>Pyrgo sp.</i>	0	0	0	0	0	0	0	0	0	0	0	0
<i>Pyrgo williamsoni</i>	0	0	2	0	0	0	0	0	0	0	0	0
<u>Quinqueloculina sp.</u>	<u>3</u>	<u>5</u>	<u>3</u>	<u>5</u>	<u>3</u>	<u>0</u>	<u>3</u>	<u>1</u>	<u>0</u>	<u>1</u>	<u>4</u>	<u>1</u>
<i>Reophax sp.</i>	0	0	0	0	0	0	0	0	0	0	0	0
<i>Sigmolopsis schlumbergeri</i>	0	0	0	0	0	0	0	0	0	0	0	0
<u>Textularia sp.</u>	<u>5</u>	<u>2</u>	<u>4</u>	<u>2</u>	<u>8</u>	<u>8</u>	<u>13</u>	<u>0</u>	<u>9</u>	<u>4</u>	<u>9</u>	<u>1</u>
<u>Trifarina angulosa</u>	<u>45</u>	<u>54</u>	<u>41</u>	<u>15</u>	<u>80</u>	<u>116</u>	<u>138</u>	<u>196</u>	<u>50</u>	<u>108</u>	<u>26</u>	<u>51</u>
<i>Triloculina tricarinata</i>	1	0	7	0	0	1	0	0	0	0	4	0
<u>Uvigerina mediterranea</u>	<u>17</u>	<u>6</u>	<u>1</u>	<u>6</u>	<u>1</u>	<u>1</u>	<u>0</u>	<u>8</u>	<u>9</u>	<u>10</u>	<u>10</u>	<u>0</u>
Total benthic foraminifera	225	234	309	237	219	249	270	495	208	241	220	202
Total planktonic foraminifera	390	508	585	65	425	323	396	500	509	687	442	350
Sample weight (mg)	148	137	138	679	169	100	45	99	68	84	177	138
Foraminifera/mg	4.2	5.4	6.5	0.4	3.8	5.7	15	10	11	11	3.7	4.0

1108 Table A3: Benthic foraminifera absolute abundances (number of individuals) and general micropaleontological data for
1109 cores 44 and 45. Species with >2% relative abundance in in at least one core (42, 43, 44, 45) in bold, >5% in bold and
1110 underlined. (Refer to Table A2 for core 42 and 43 data.)

Cm (bsf)	Core 44								Core 45					
	5	27	46	80	120	139	180	223	31	57	94	142	209	254
Species	Individuals								Individuals					
<i>Amphicoryna scalaris</i>	2	1	1	0	0	0	0	0	0	2	0	0	0	0
<i>Bigenerinanosaria</i>	2	2	2	0	1	0	0	0	4	6	1	0	0	1
<i>Buccella frigida</i>	0	0	0	0	0	0	0	0	0	0	0	0	0	0
<i>Bulimina elongata</i>	0	0	0	0	0	1	0	0	0	0	0	0	0	0
<u>Bulimina gibba</u>	4	0	6	5	12	10	7	8	2	3	13	8	11	3
<u>Bulimina marginata</u>	43	29	20	6	7	5	6	4	65	69	6	9	11	10
<i>Bulivina sp.</i>	10	9	3	2	3	10	4	4	17	7	7	6	5	2
<u>Cassidulina laevigata</u>	77	47	30	12	20	14	23	13	79	55	23	19	34	23
<i>Cassidulina obtuse</i>	9	5	3	2	3	1	2	3	5	1	3	2	5	8
<u>Cassidulina reniforme</u>	0	0	1	8	5	7	4	11	0	11	14	5	9	6
<u>Cibicides lobatula</u>	51	32	52	63	77	87	82	66	26	27	38	54	58	69
<u>Cibicides refulgens</u>	5	2	13	7	3	20	14	7	7	12	18	16	19	4
<i>Cibicoides pachyderma</i>	1	0	0	0	1	0	0	0	2	0	0	1	0	0
<i>Dentalina subsoluta</i>	0	0	0	0	0	0	0	0	0	0	0	0	0	0
<u>Discanomalina coronata</u>	1	1	5	9	5	8	2	5	3	2	1	4	10	8
<i>Eggerella bradyi</i>	0	1	0	0	0	0	1	0	0	0	0	0	0	0
<u>Elphidium excavatum clavatum</u>	0	0	1	10	5	8	6	7	0	6	8	5	9	9
<i>Elphidium excavatum selseyensis</i>	0	5	4	2	0	1	1	1	2	3	4	6	6	4
<i>Fissurina sp.</i>	0	2	0	0	0	0	0	0	3	0	0	0	0	0
<i>Gavelinopsis translucens</i>	0	0	0	0	0	0	0	0	0	0	0	0	0	0
<u>Globocassidulina subglobosa</u>	0	0	1	2	0	2	1	0	0	0	1	3	2	0
<i>Guttulina sp.</i>	0	0	0	0	0	0	0	0	0	1	0	0	1	0
<u>Gyroidinoides soldanii</u>	0	0	2	0	0	1	0	0	0	0	2	0	3	0
<i>Hyalinea balthica</i>	0	0	1	0	0	1	0	0	2	0	0	0	0	0
<i>Lagena sp.</i>	0	0	0	0	0	0	0	0	0	0	0	0	2	0
<i>Lagena striata</i>	1	0	0	0	0	0	0	0	2	0	1	0	1	1
<u>Lenticulina sp.</u>	2	3	3	3	1	2	1	5	0	1	1	2	0	0
<u>Melonis barleeanus</u>	2	1	2	1	3	4	4	7	7	5	7	8	7	1
<i>Miliammina fusca</i>	0	1	1	3	0	0	0	2	1	0	0	1	1	0
<i>Miliolinella chukchiensis</i>	0	0	0	0	0	0	0	0	0	0	0	0	0	1
<i>Nonionella turgida</i>	0	0	0	0	0	0	1	0	0	0	0	0	0	0
<i>Oolina caudigera</i>	0	0	0	0	0	0	0	2	0	0	0	0	0	0
<u>Planulina ariminensis</u>	27	18	13	4	1	4	1	3	23	11	3	3	8	1
<i>Pyrgo sp.</i>	0	0	0	0	0	0	0	0	0	6	0	0	0	0
<i>Pyrgo williamsoni</i>	0	0	0	1	0	0	2	0	0	0	0	0	0	0
<u>Quinqueloculina sp.</u>	0	0	2	4	2	5	3	4	0	0	3	4	7	6
<i>Reophax sp.</i>	0	0	0	0	1	0	0	1	0	0	3	0	0	1
<i>Sigmoilopsis schlumbergeri</i>	0	0	0	0	2	3	1	2	0	1	1	4	4	1
<u>Textularia sp.</u>	24	19	11	3	6	6	5	2	15	13	2	3	0	5
<u>Trifarina angulosa</u>	45	33	28	46	33	46	37	39	52	36	38	41	48	50
<i>Triloculina tricarinata</i>	0	0	0	1	0	0	0	0	0	0	0	1	0	0
<u>Uvigerina mediterranea</u>	67	40	38	6	13	16	14	7	105	53	6	13	10	12
Total benthic foraminifera	371	250	242	200	204	262	222	203	422	329	204	218	271	226
Total planktonic forams.	477	387	315	259	187	285	255	207	485	315	195	263	287	215
Sample weight (mg)	83	88	105	143	100	84	162	160	82	99	132	152	186	144
Foraminifera/mg	10	7.3	5.3	3.2	3.9	6.5	2.9	2.6	11	6.5	3.0	3.2	3.0	3.1

Figure
[Click here to download high resolution image](#)

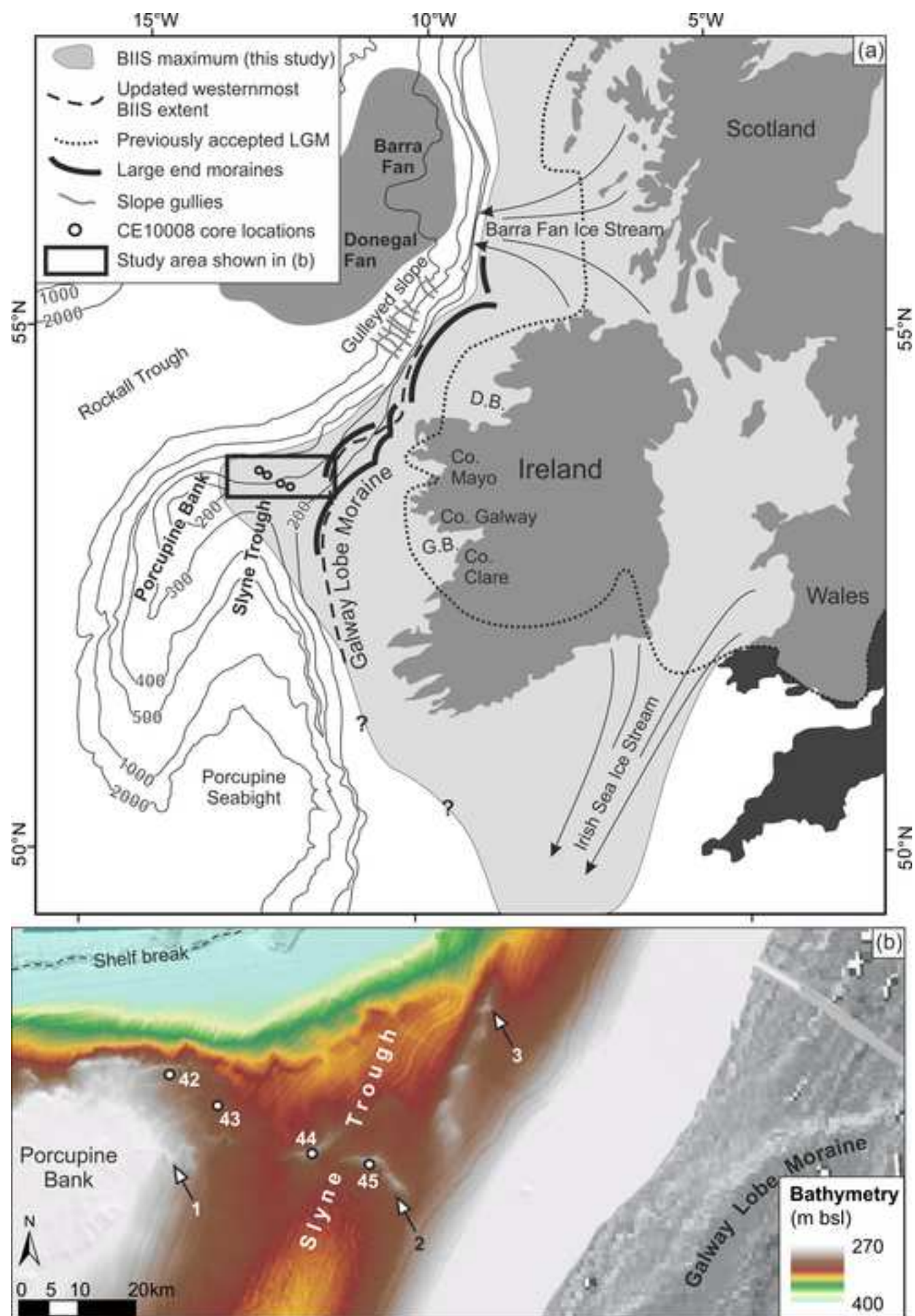


Figure
[Click here to download high resolution image](#)

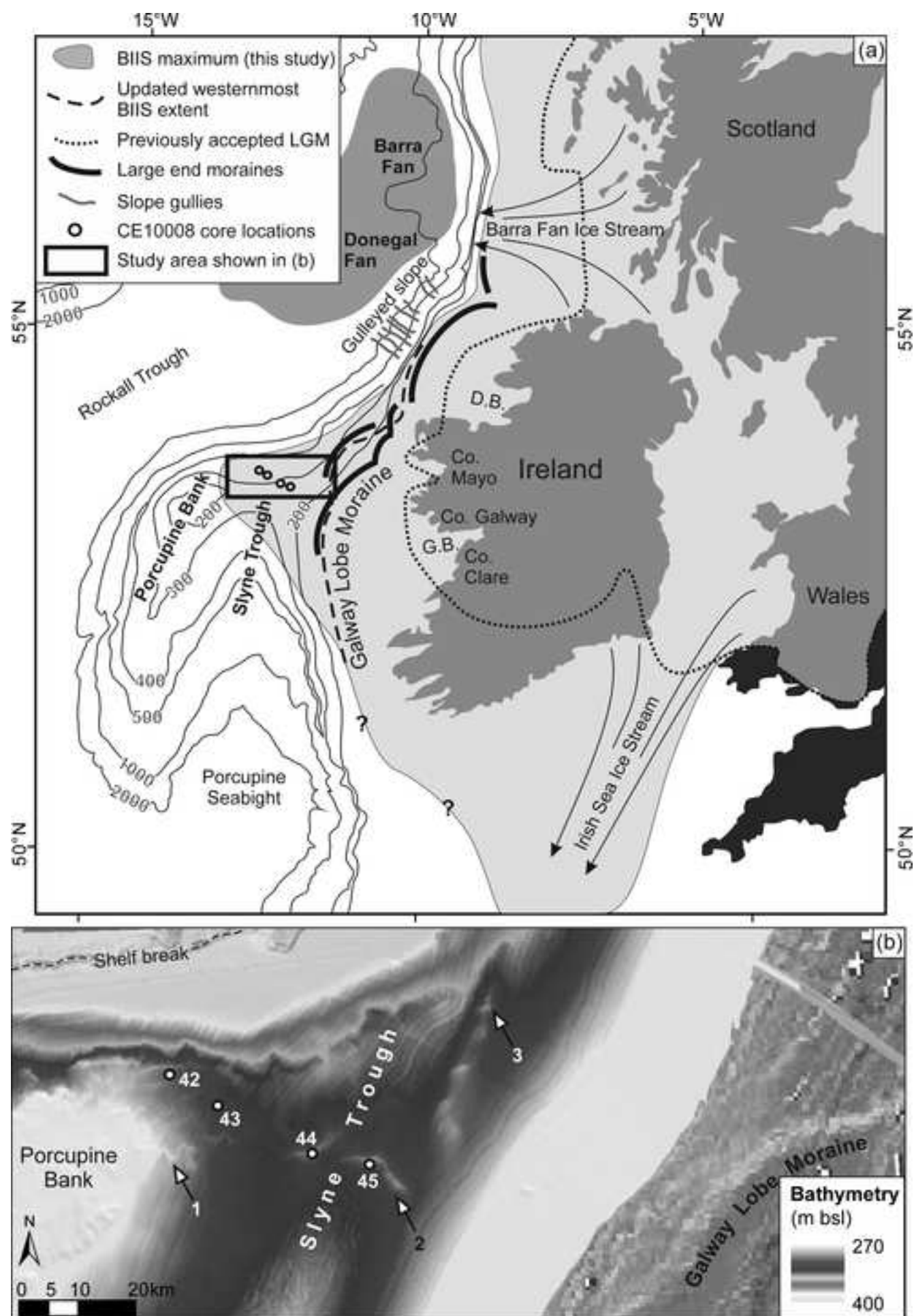


Figure
[Click here to download high resolution image](#)

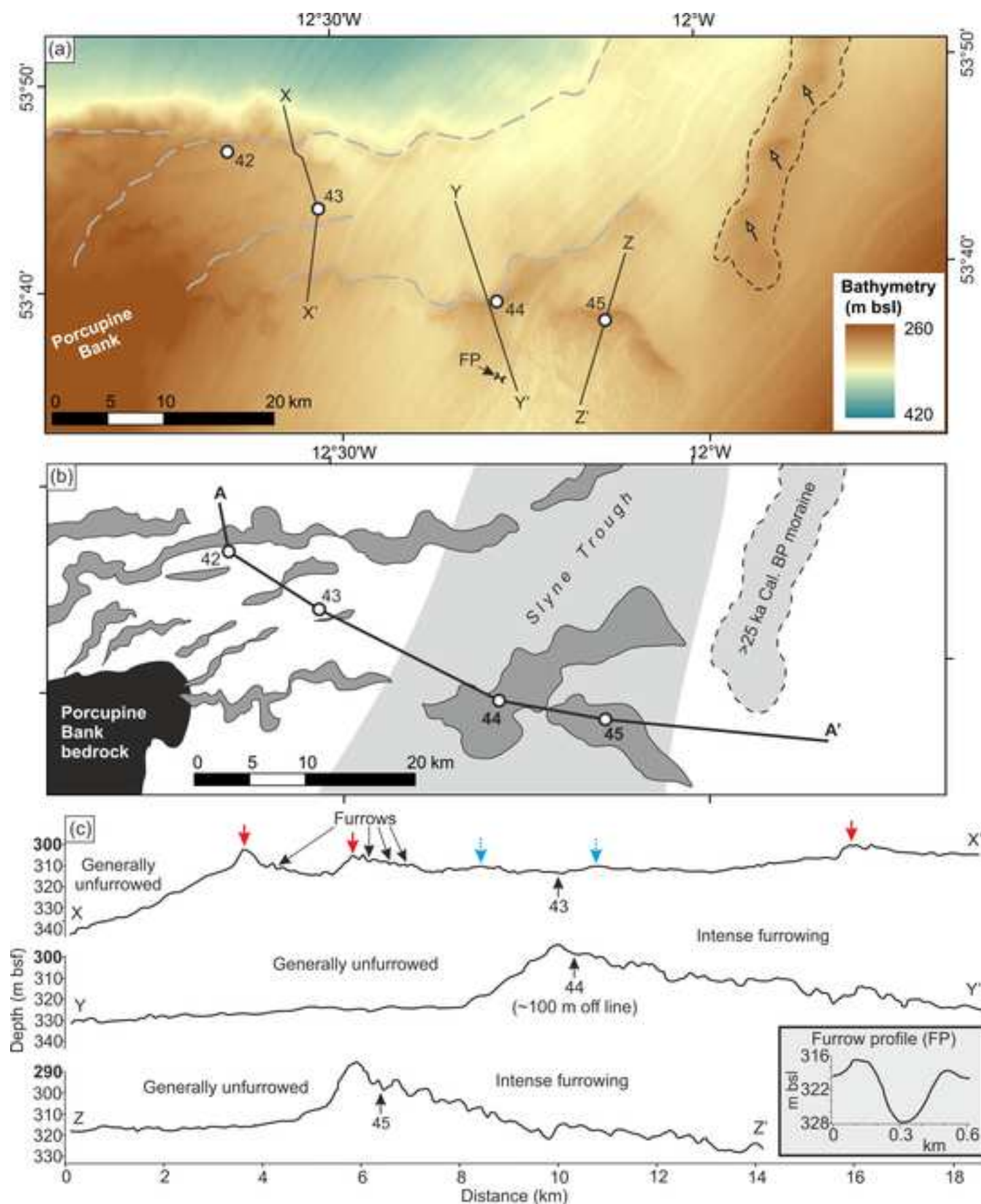


Figure
[Click here to download high resolution image](#)

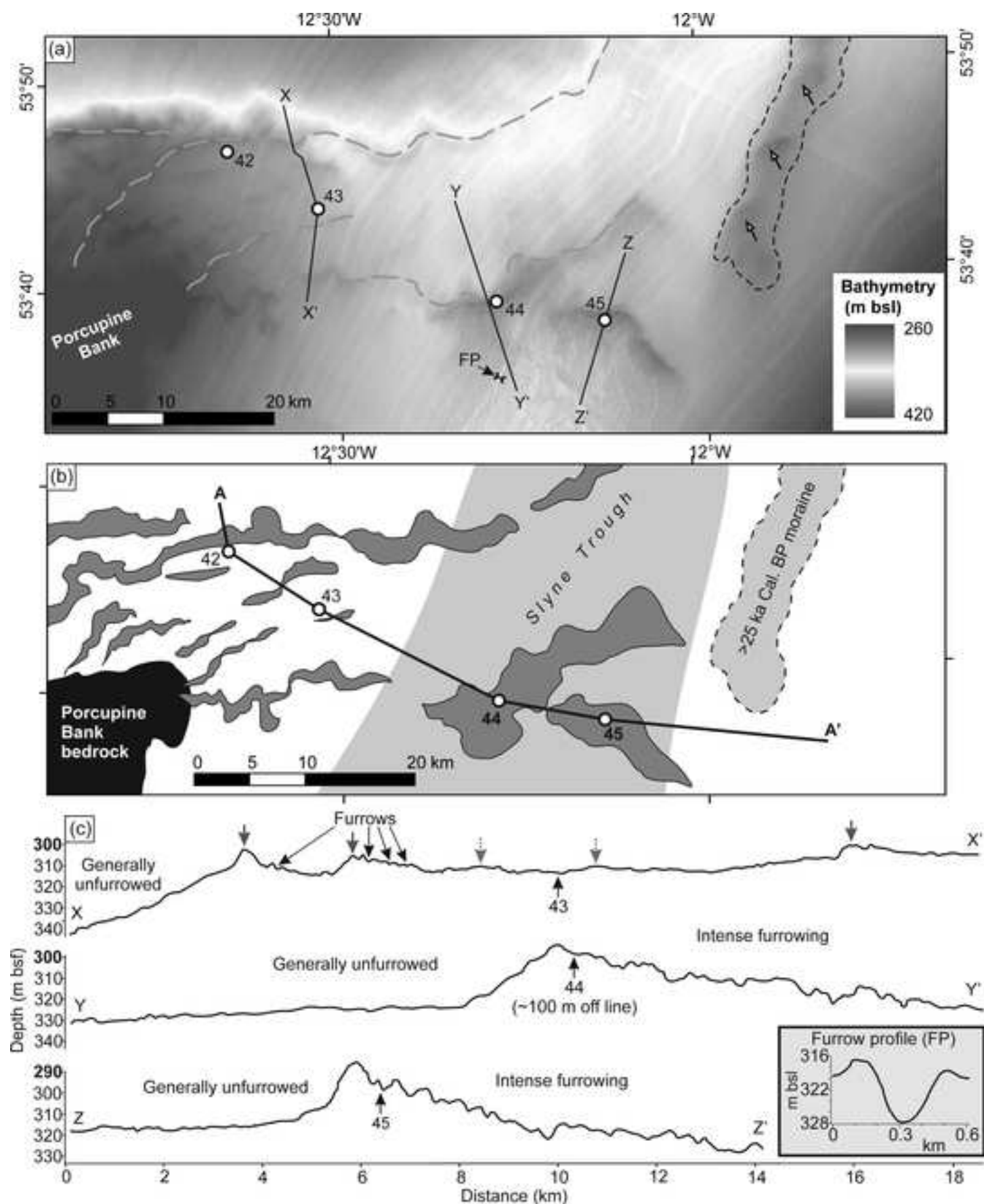
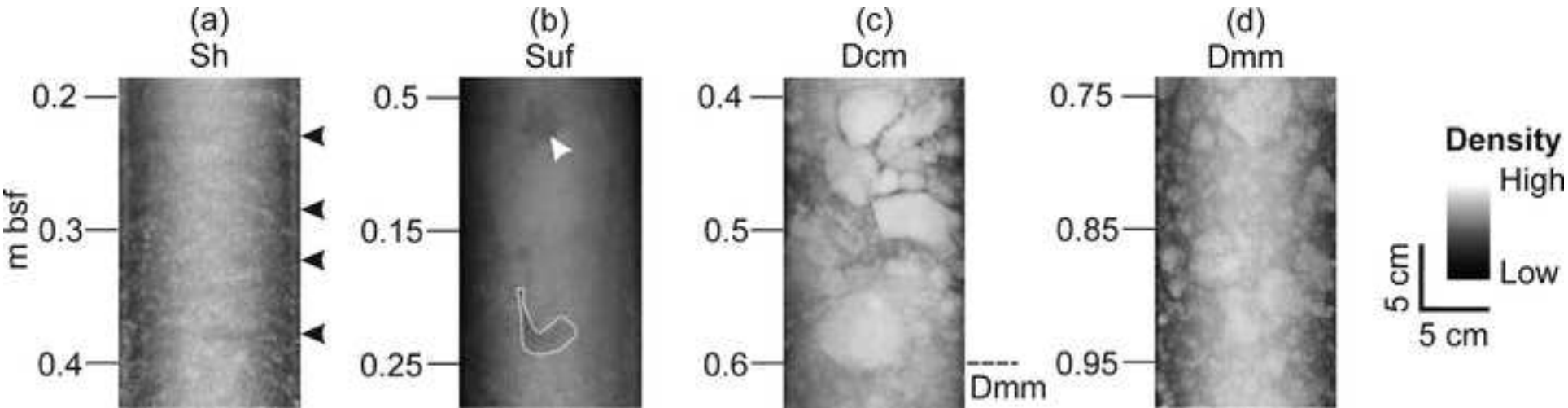
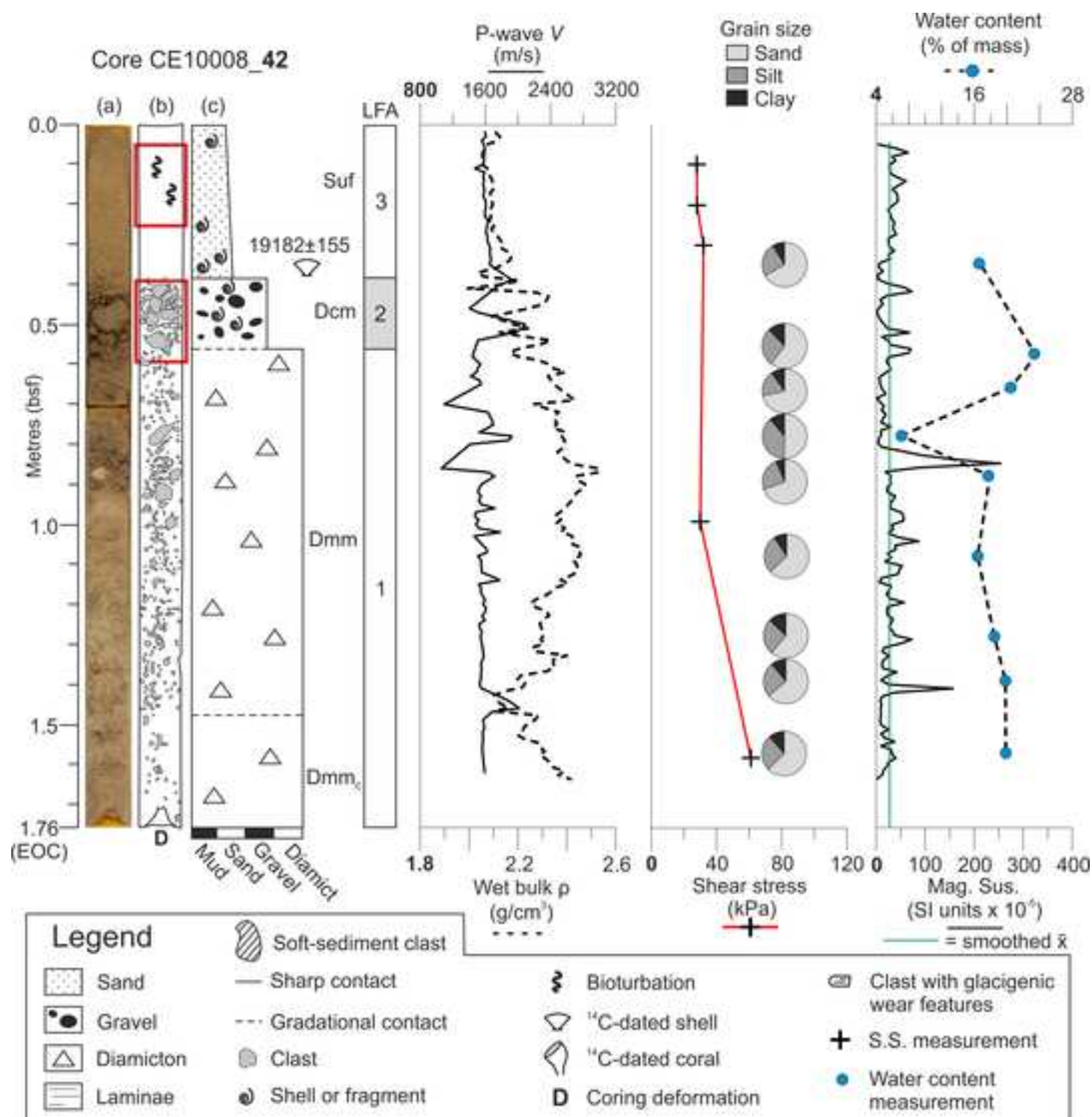


Figure
[Click here to download high resolution image](#)



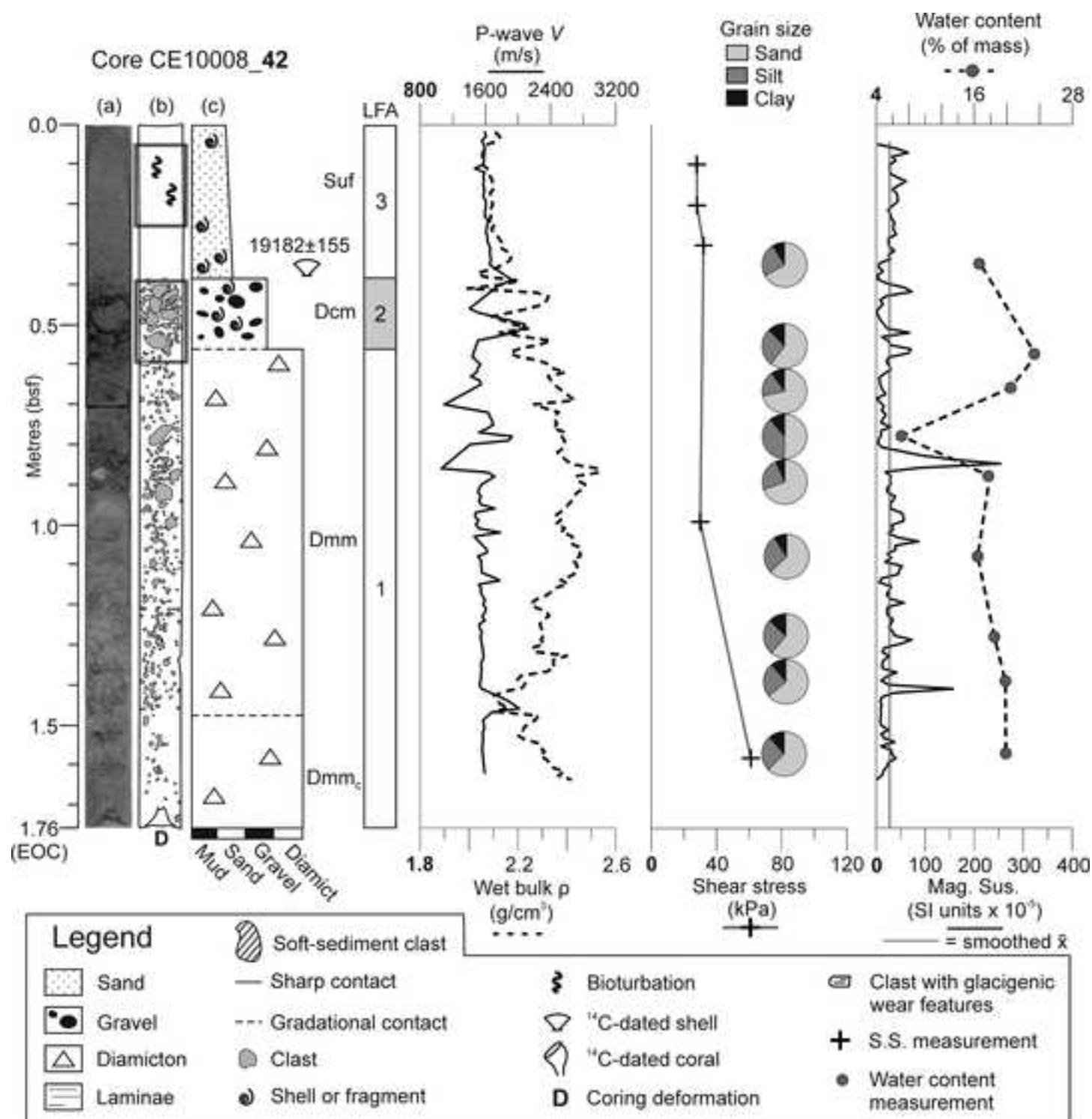
Figure

[Click here to download high resolution image](#)



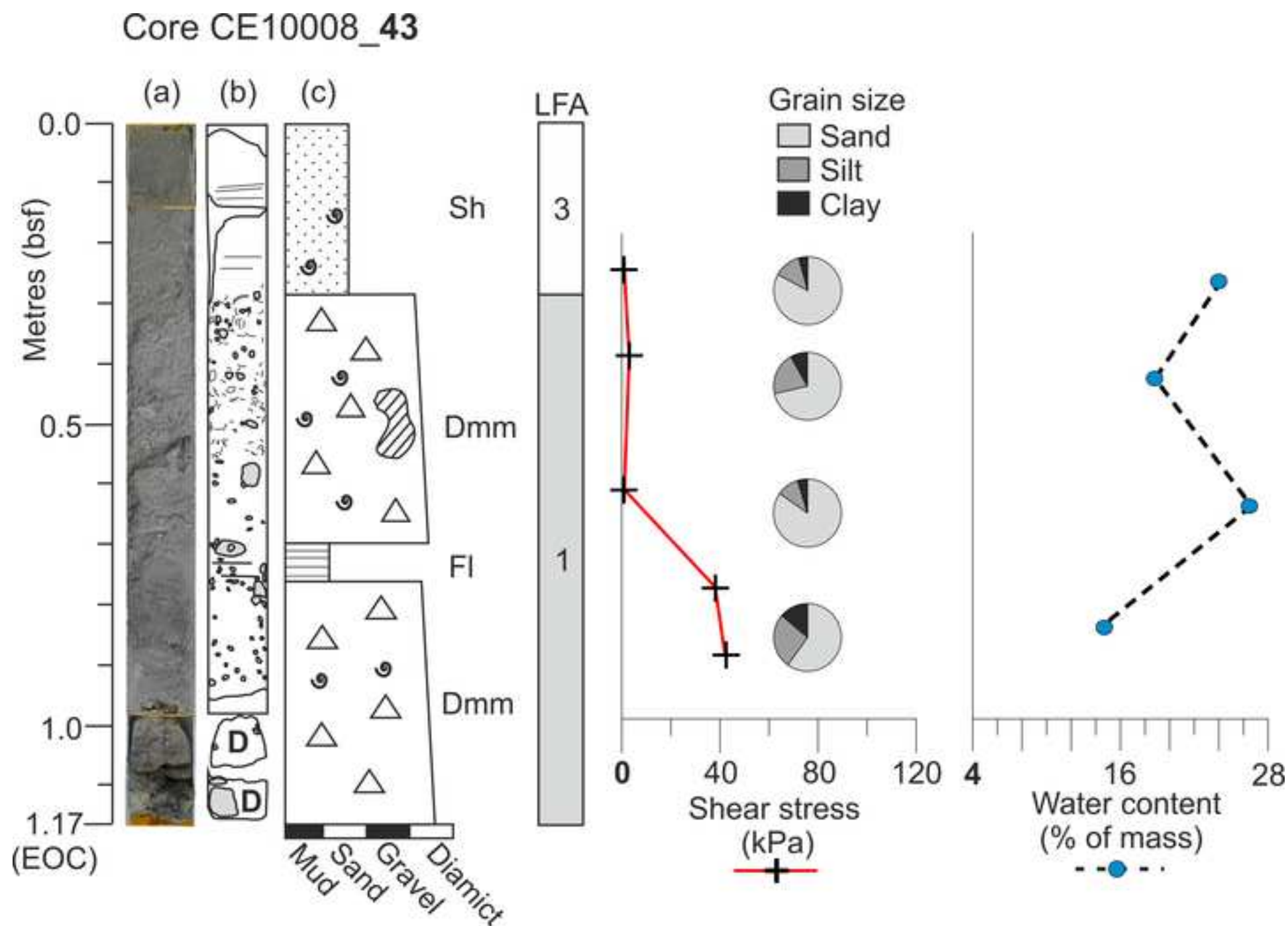
Figure

[Click here to download high resolution image](#)



Figure

[Click here to download high resolution image](#)



Figure

[Click here to download high resolution image](#)

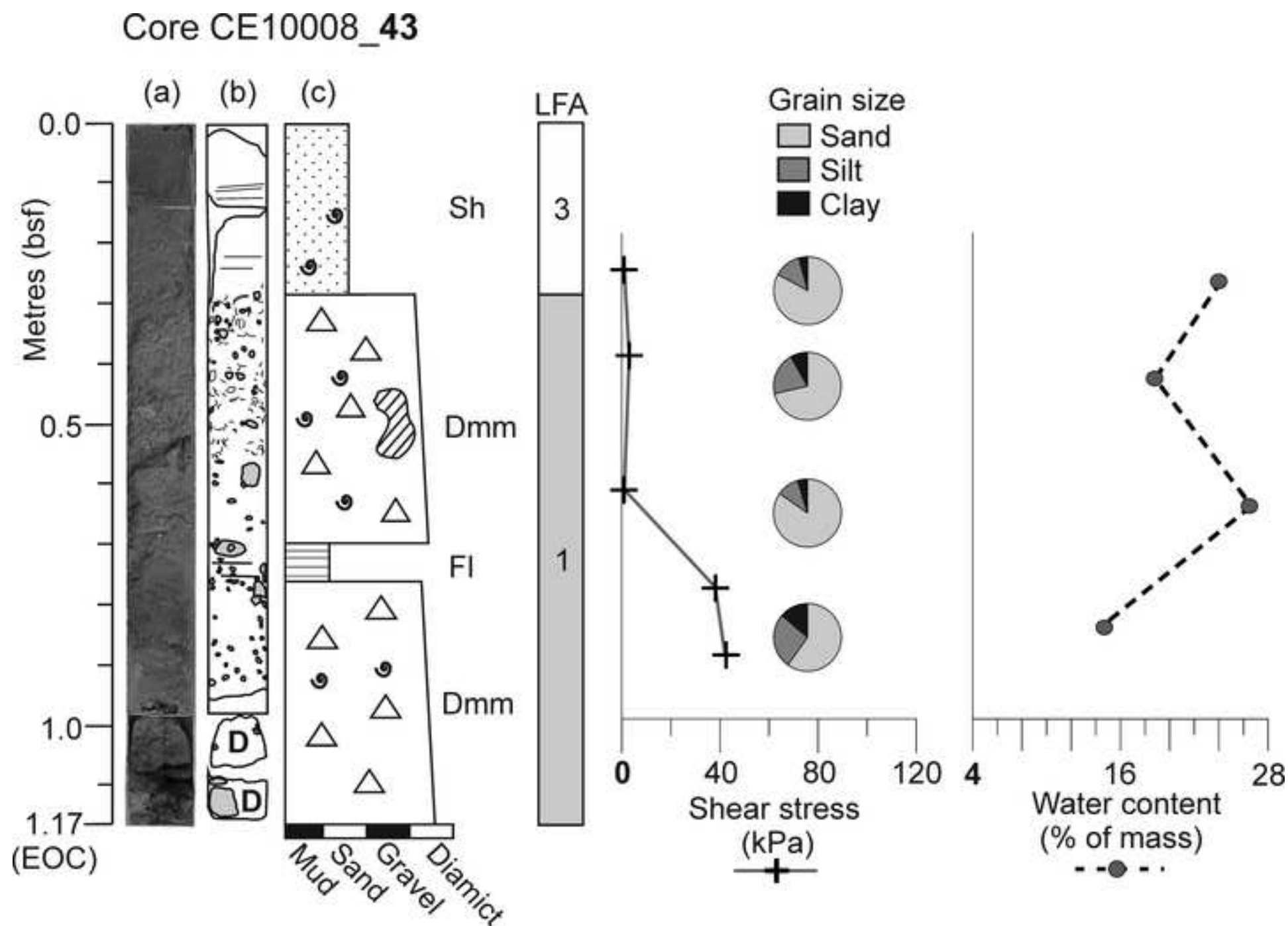


Figure
[Click here to download high resolution image](#)

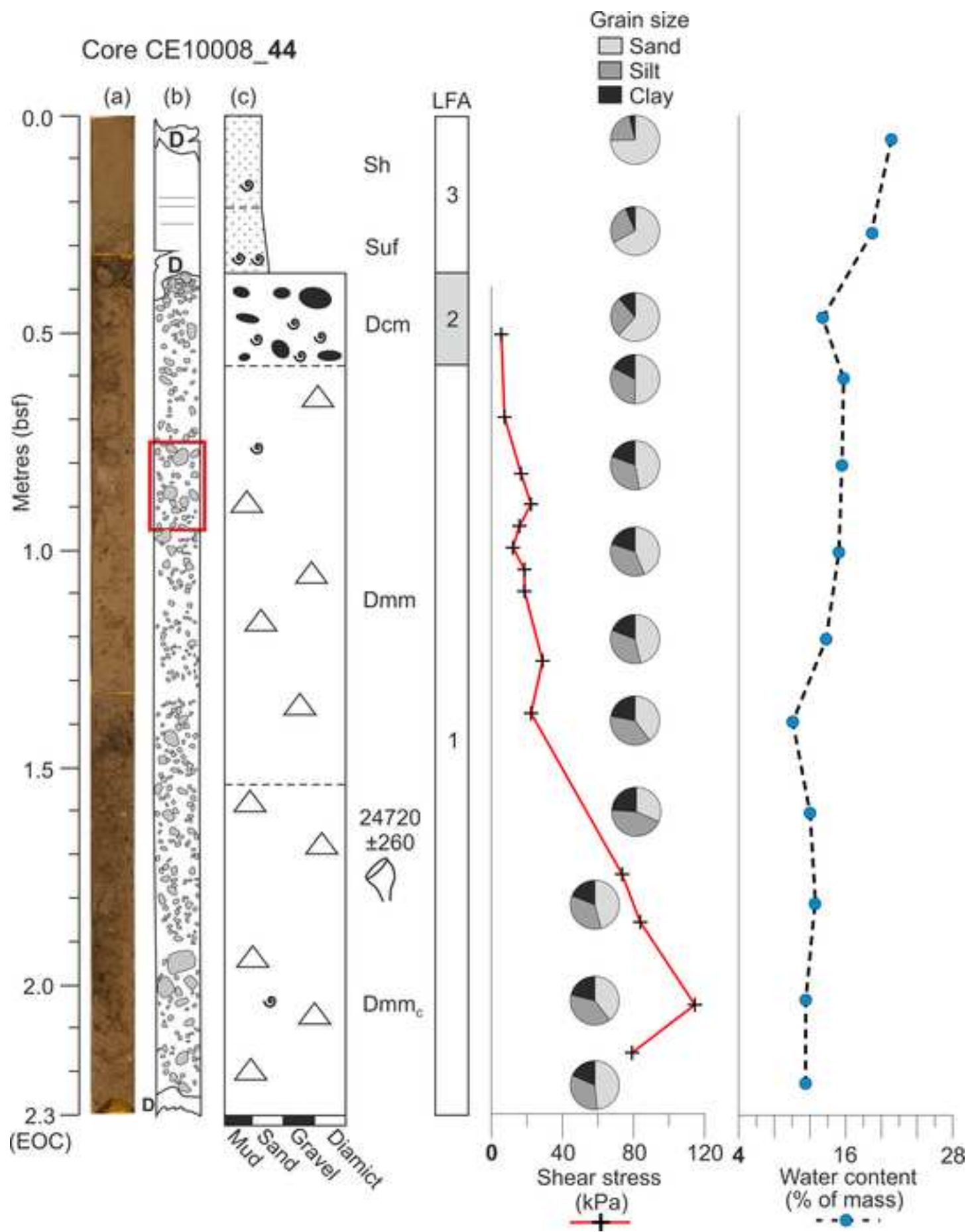


Figure
[Click here to download high resolution image](#)

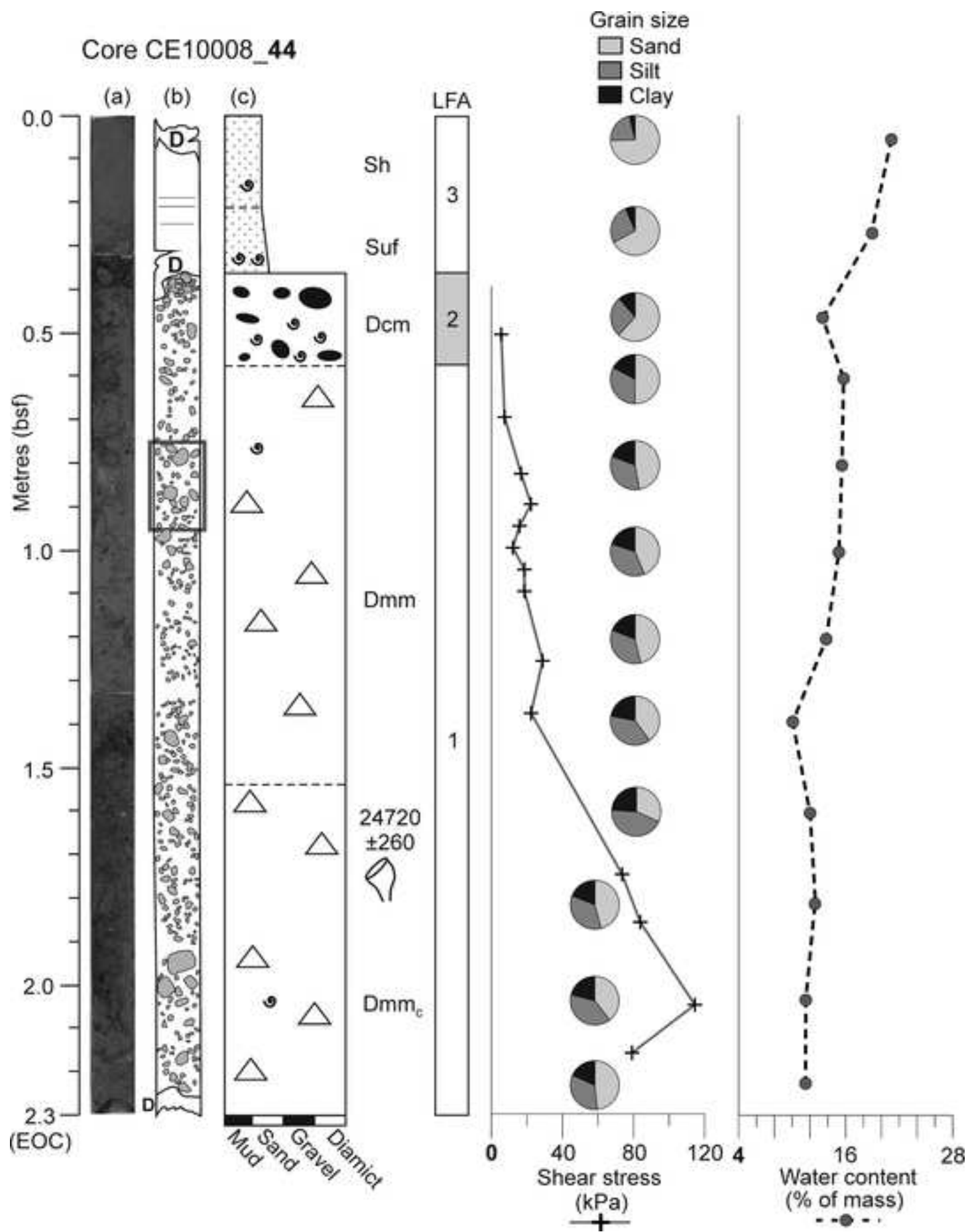


Figure
[Click here to download high resolution image](#)

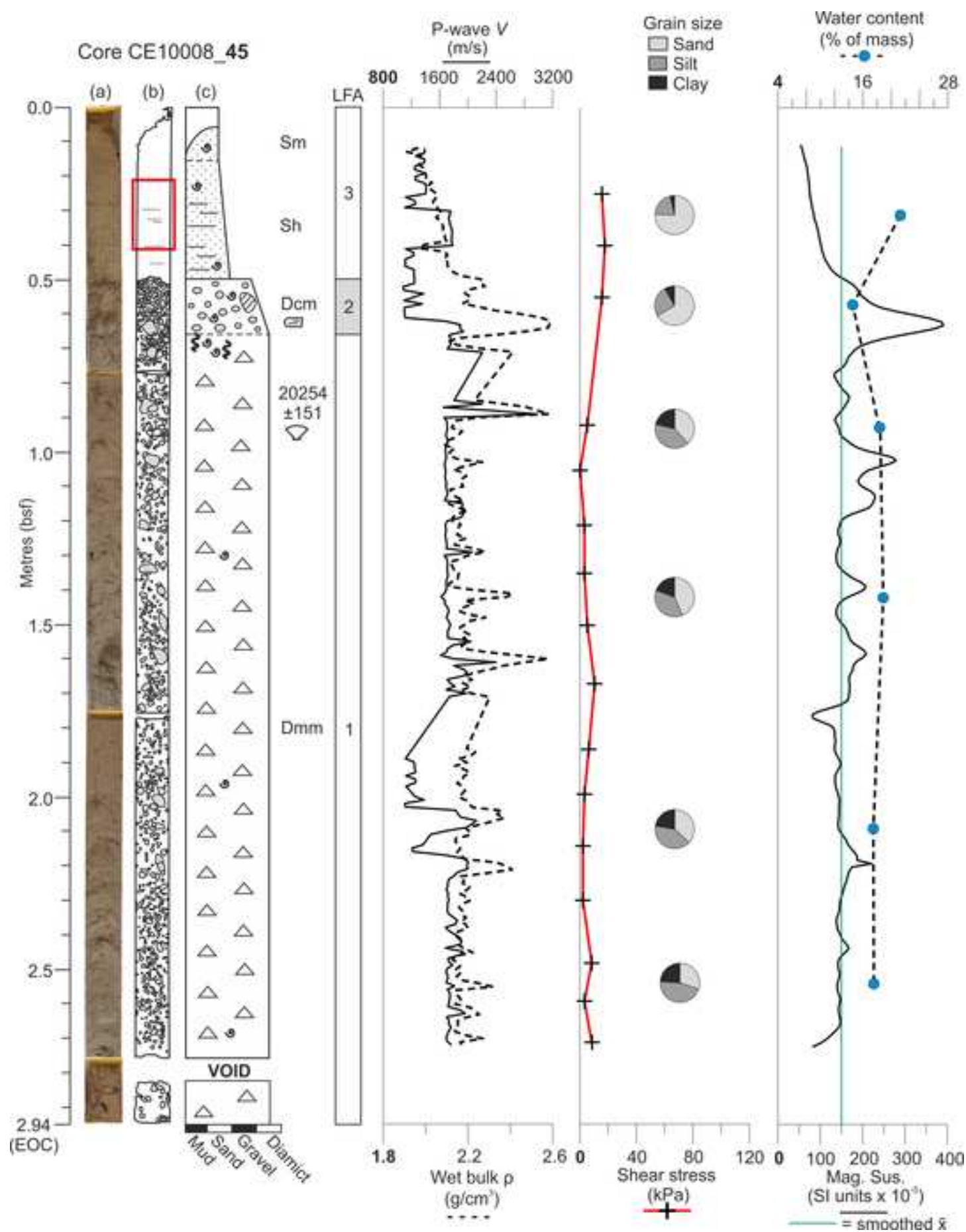


Figure
[Click here to download high resolution image](#)

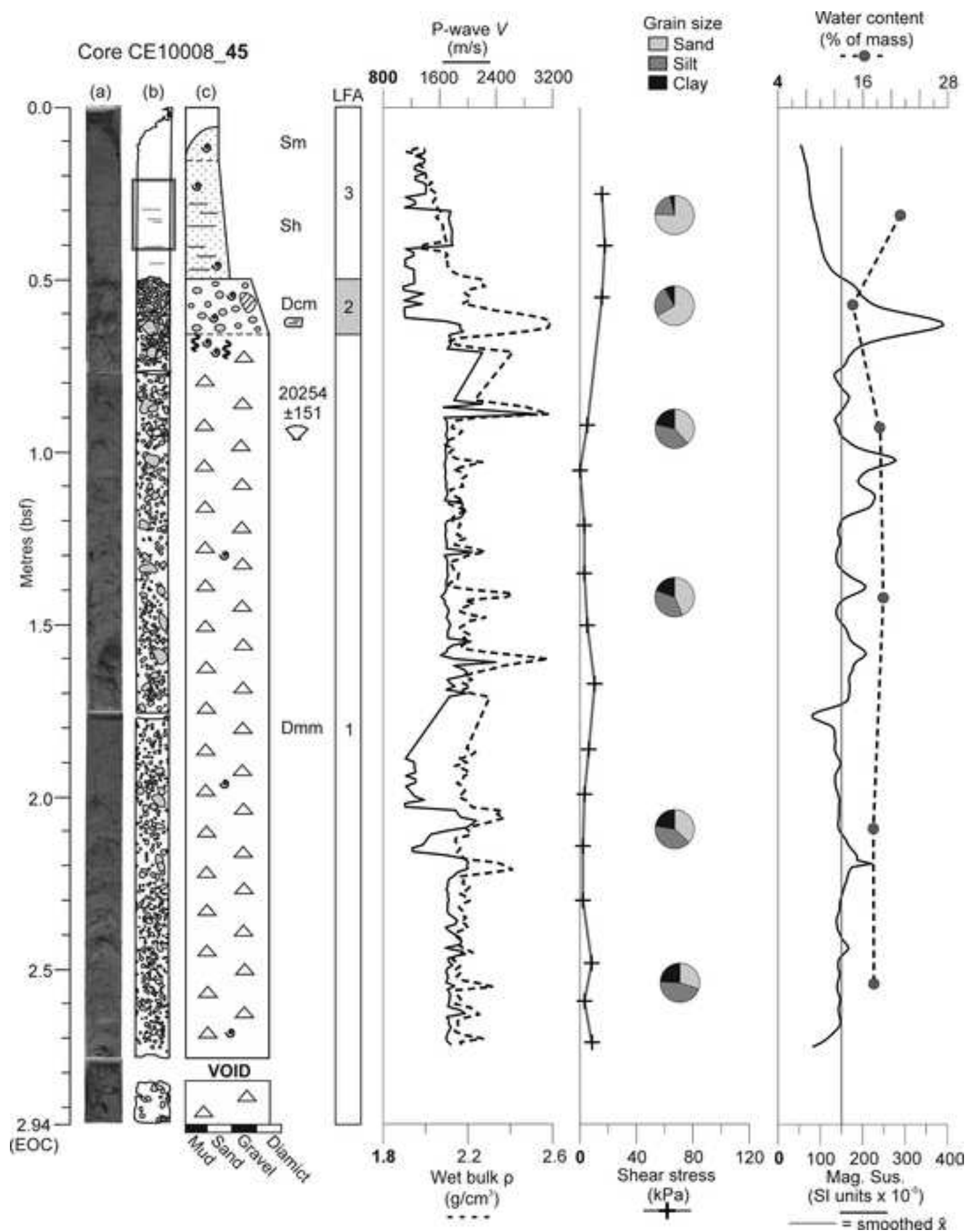


Figure
[Click here to download high resolution image](#)

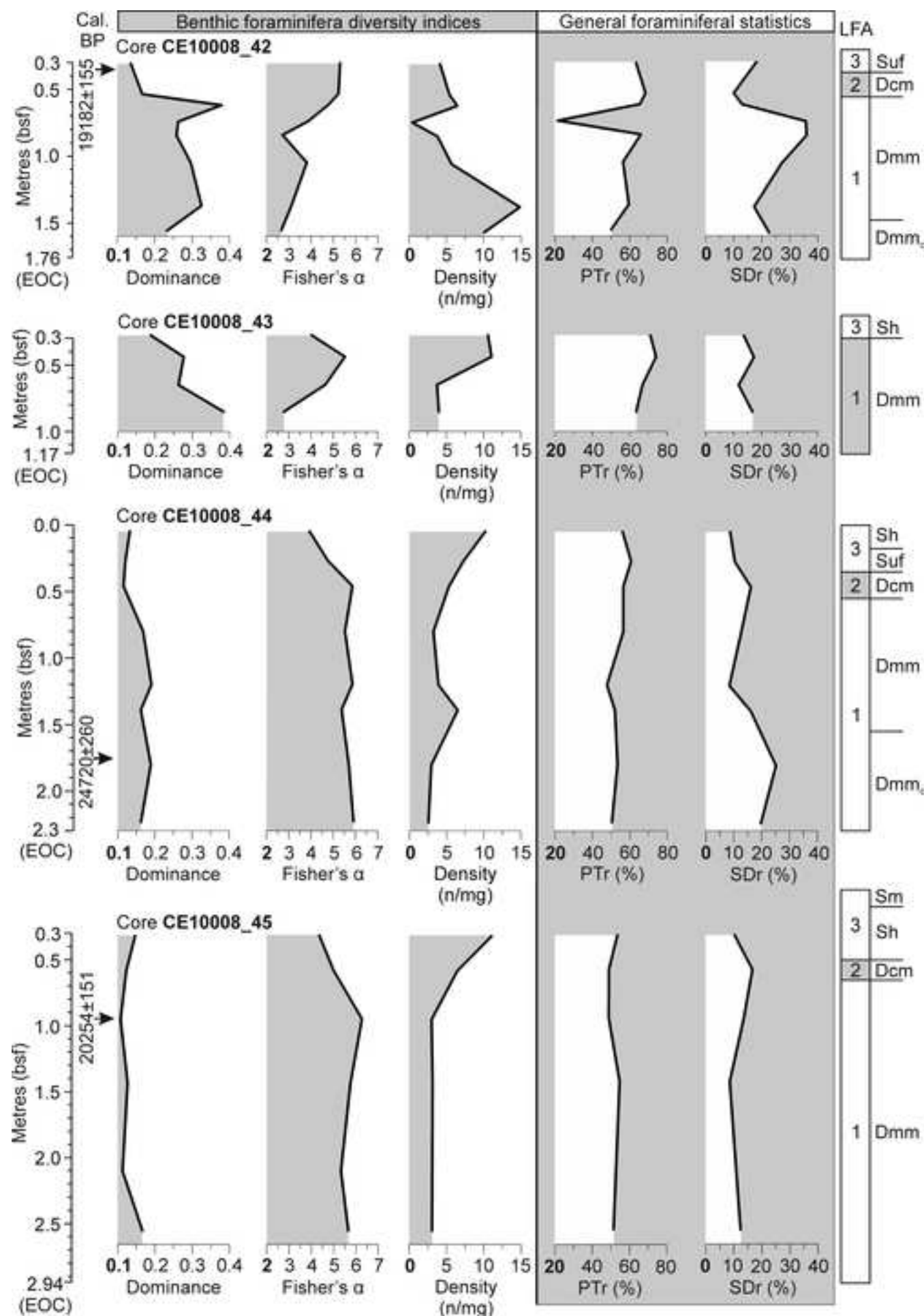


Figure
[Click here to download high resolution image](#)

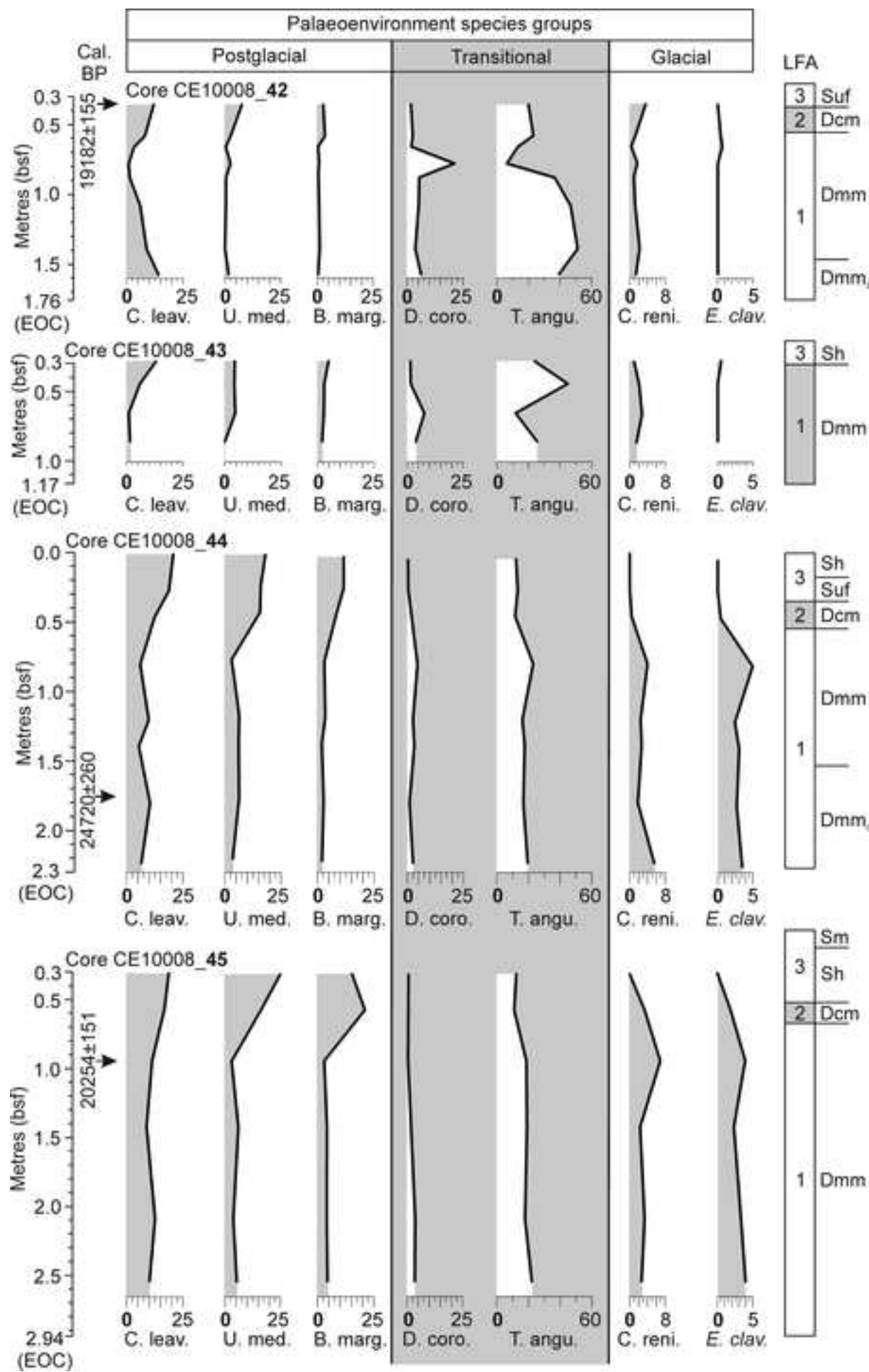


Figure
[Click here to download high resolution image](#)

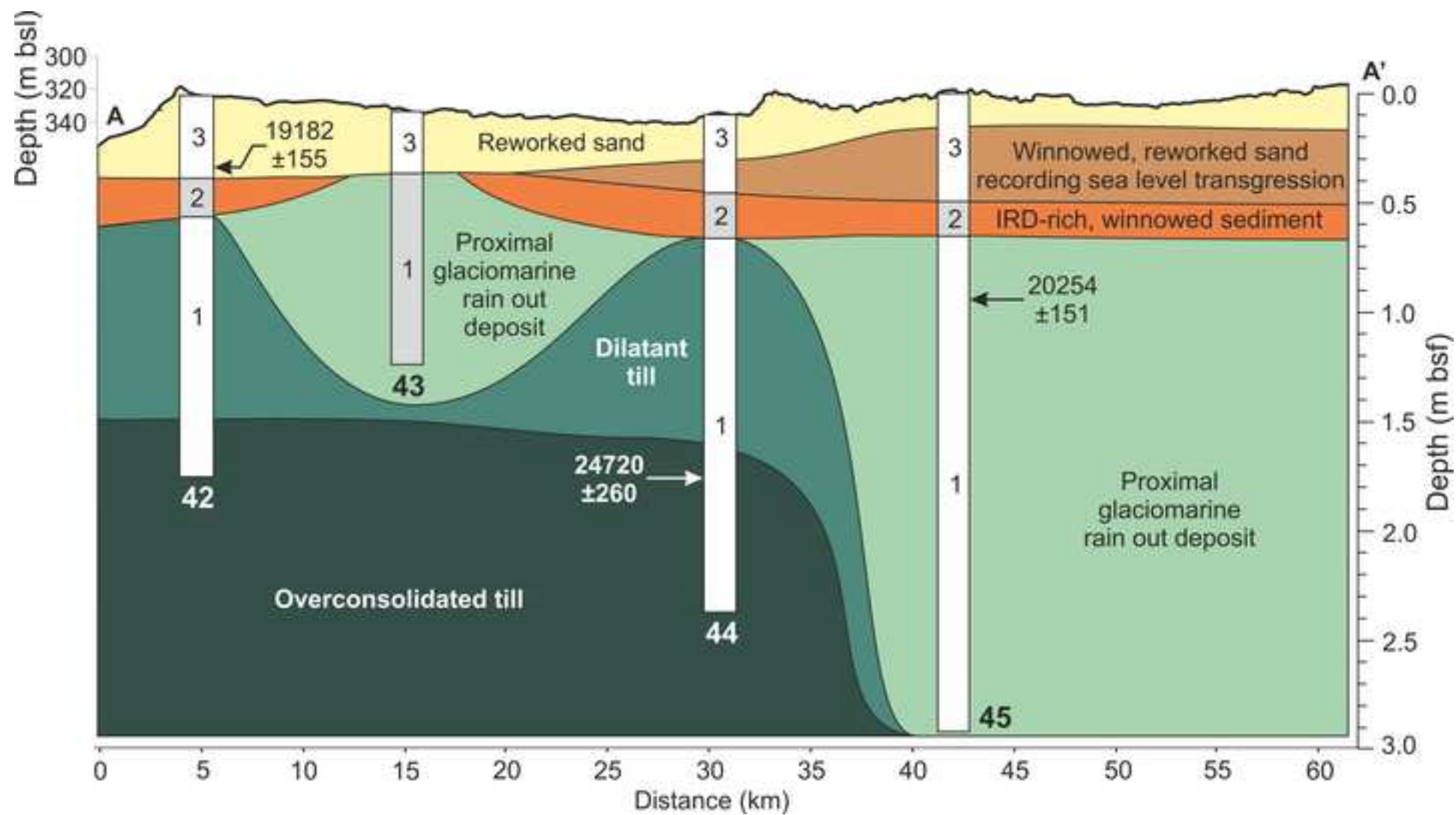
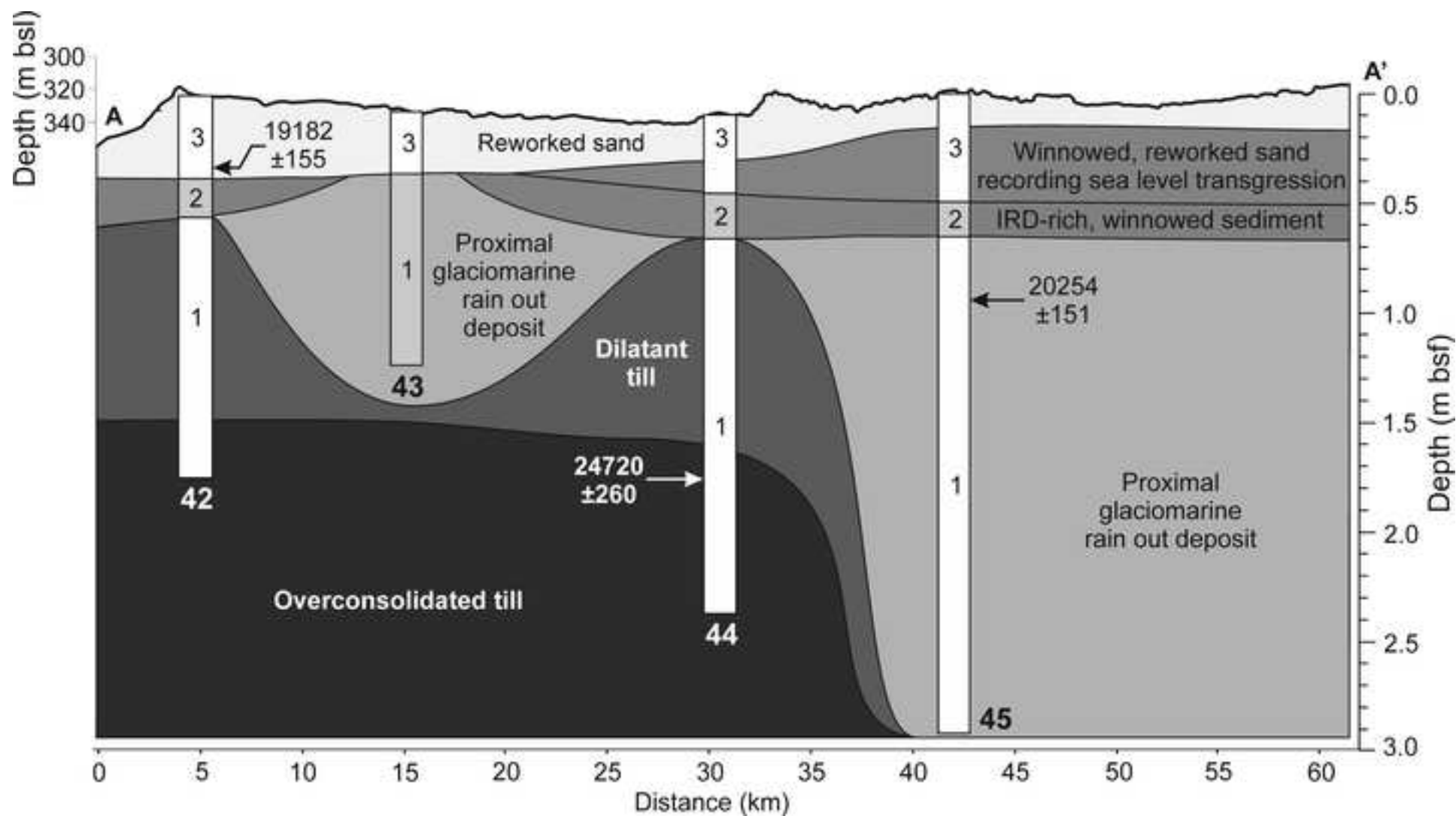
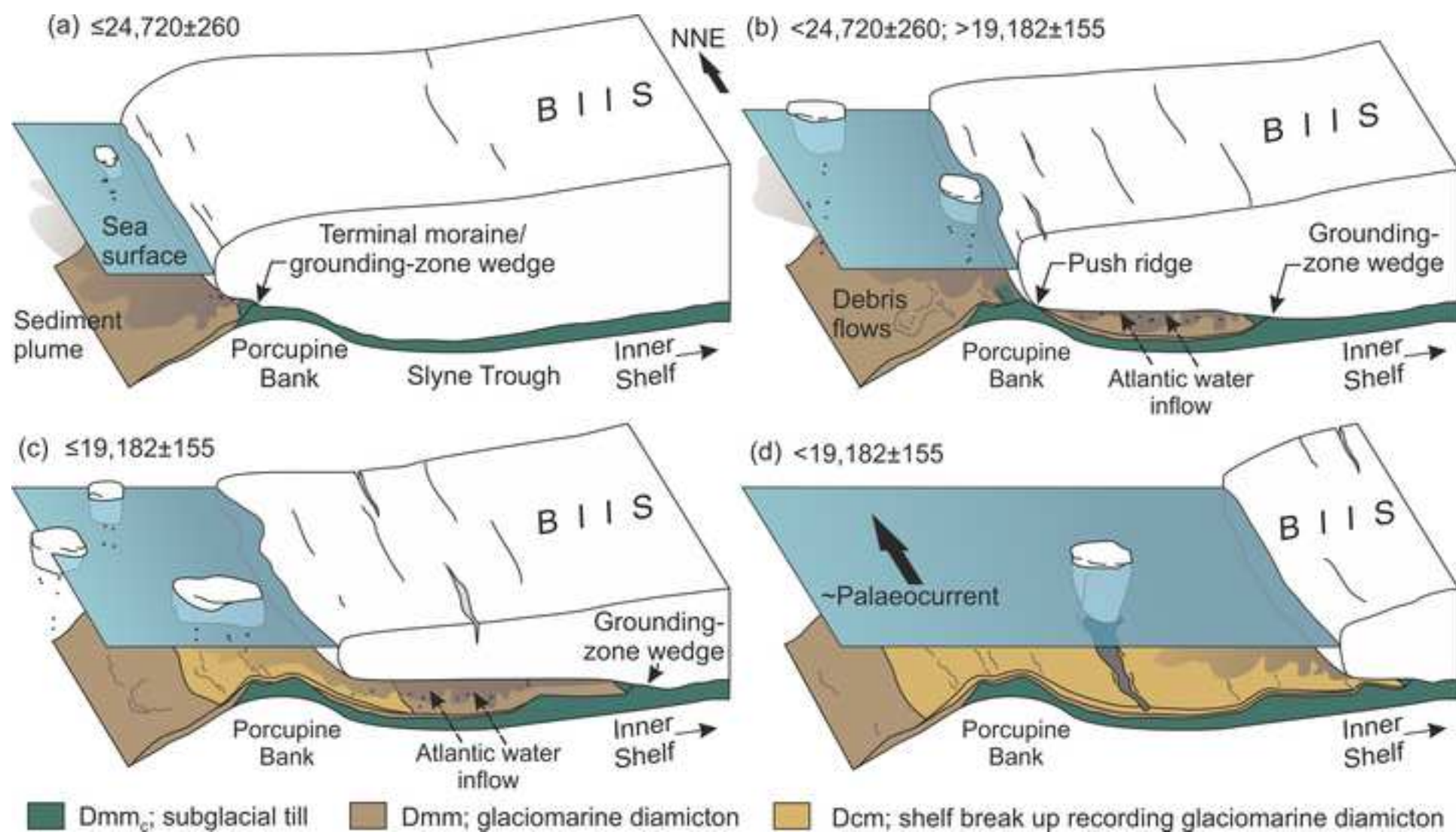


Figure
[Click here to download high resolution image](#)



Figure

[Click here to download high resolution image](#)



Figure

[Click here to download high resolution image](#)

